The extended cytoplasmic tail of the human B4GALNT2 is critical for its Golgi targeting and post-Golgi sorting

Sophie Groux-Degroote, Céline Schulz, Virginie Cogez, Maxence Noel, Lucie Portier, Dorothée Vicogne, Carlos Solórzano, Fabio Dall'Olio, Agata Steenackers, Marlène Mortuaire, et al.

The FEBS Journal

FEBS PRESS science publishing by scientists

The extended cytoplasmic tail of the human B4GALNT2 is critical for its Golgi targeting and post-Golgi sorting

Sophie Groux-Degroote[1], Céline Schulz[1,2], Virginie Cogez[1], Maxence Noël[1], Lucie Portier[1], Dorothée Vicogne[1], Carlos Solorzano[1], Fabio Dall'Olio[3], Agata Steenackers[1], Marlène Mortuaire[1], Mariano Gonzalez-Pisfil[2], Mélanie Henry[2], François Foulquier[1], Laurent Héliot[2] and Anne Harduin-Lepers[1]

1 Univ. Lille, CNRS, UMR 8576 - UGSF - Unité de Glycobiologie Structurale et Fonctionnelle, Lille, France
2 Univ. Lille, CNRS, UMR 8523 – PhLAM - Laboratoire de Physique des Lasers, Atomes, Molécules, Lille, France
3 Department of Experimental, Diagnostic and Specialty Medicine (DIMES), University of Bologna, Italy

Keywords
B4GALNT2; cytoplasmic tail; glycosyltransferase localization; Golgi; vesicles

Correspondence
A. Harduin-Lepers, Unité de Glycobiologie Structurale et Fonctionnelle, UMR CNRS 8576, Université Lille Nord de France, Lille1, 59655 Villeneuve d'Ascq, France
Fax: +33 320 43 65 55
Tel: +33 320 33 62 46
E-mail: anne.harduin-lepers@univ-lille.fr

Sophie Groux-Degroote, Céline Schulz and Virginie Cogez contributed equally to the work.

(Received 15 January 2018, revised 15 June 2018, accepted 31 July 2018)

doi:10.1111/febs.14621

The Sd^a/Cad antigen reported on glycoconjugates of human tissues has an increasingly recognized wide impact on the physio-pathology of different biological systems. The last step of its biosynthesis relies on the enzymatic activity of the β1,4-N-acetylgalactosaminyltransferase-II (B4GALNT2), which shows the highest expression level in healthy colon. Previous studies reported the occurrence in human colonic cells of two B4GALNT2 protein isoforms that differ in the length of their cytoplasmic tail, the long isoform showing an extended 66-amino acid tail. We examined here, the subcellular distribution of the two B4GALNT2 protein isoforms in stably transfected colonic LS174T cells and in transiently transfected HeLa cells using fluorescence microscopy. While a similar subcellular distribution at the *trans*-Golgi cisternae level was observed for the two isoforms, our study pointed to an atypical subcellular localization of the long B4GALNT2 isoform into dynamic vesicles. We demonstrated a critical role of its extended cytoplasmic tail for its Golgi targeting and post-Golgi sorting and highlighted the existence of a newly described post-Golgi sorting signal as well as a previously undescribed fate of a Golgi glycosyltransferase.

Database
The proteins β1,4GalNAcT II, β1,4-GalT1, FucT I, FucT VI and ST3Gal IV are noted B4GALNT2, B4GALT1, FUT1, FUT6 and ST3GAL4, whereas the corresponding human genes are noted *B4GALNT2*, *B4GALT1*, *FUT1*, *FUT6* and *ST3GAL4* according to the HUGO nomenclature.

Introduction

Glycosylation takes place along the secretory pathway and is one of the most important and complex co- and post-translational modification of proteins described in eukaryotic cells. In the Golgi apparatus, terminal glycosylation reactions (i.e., sialylation, fucosylation, *N*-acetylgalactosaminylation) generate a huge panel of glycans that confer a variety of structural and functional roles to the glycoproteins exposed at the cell

Abbreviations
CT, cytoplasmic tail; CTS, cytoplasmic/transmembrane/stem domain; eGFP, Green fluorescent protein; Fuc, Fucose; Gal, Galactose; GalNAc, *N*-acetylgalactosamine; GlcNAc, *N*-acetylglucosamine; LF-B4GALNT2, Long B4GALNT2 protein isoform; mCy, mCherry; Neu5Ac, *N*-acetylneuraminic acid; PBS, Phosphate buffer saline; SDS/PAGE, sodium dodecylsulfate polyacrylamide gel electrophoresis; SF-B4GALNT2, Short B4GALNT2 protein isoform.

surface. Besides, altered terminal glycosylation is a common feature of cancer cells conferring new phenotypic properties to the cells. Among sialylated glycans of interest, the Sd^a/Cad histo-blood group antigen (Neu5Acα2,3[GalNAcβ1,4]Galβ1,3/4GlcNAc/GalNAc) has been reported on glycoproteins and glycolipids in various biological systems [1–3]. Several studies reported this sialylated glycotope mainly in the healthy digestive tract and its disappearance in the cancerous colonic cells to the benefit of sialyl Lewis x antigen (Neu5Acα2,3Galβ1,4[Fucα1,3]GlcNAc), a selectin ligand serving as a cell adhesion molecule [4,5]. The last biosynthetic step of the Sd^a/Cad antigen is ensured by a glycosyltransferase named B4GALNT2 (alias β1,4GalNAcT-II or GALGT2) that was cloned from human colonic Caco-2 cells [6,7]. Interestingly, we have shown that the human *B4GALNT2* gene possesses two alternative first exons giving rise to two transcripts and two potential protein isoforms one of which displaying an unusual extended cytoplasmic tail (CT) of 66 amino acid residues. The two predicted B4GALNT2 protein isoforms possess identical transmembrane, stem, and catalytic domains, but different N termini. As a first step to decipher the regulatory mechanisms underpinning Sd^a/Cad expression in the human colon, a seminal and comprehensive study was carried out in human cultured cells and biopsies. We recently showed that transcriptional regulation of *B4GALNT2* was the main regulatory mechanisms underlying Sd^a/Cad expression in the digestive tract [8]. The major transcript variant was found to be the short transcript, largely expressed in embryonic colonic cells CcD841CoN, healthy colon, and stomach, and downregulated in these tumor tissues. Using western blotting approaches and a commercial polyclonal antibody directed against the common stem region of the two isoforms, this previous study also established the presence of the two predicted B4GALNT2 protein isoforms in healthy colon samples and colonic cells designated short protein isoform (SF-B4GALNT2) and long protein isoform (LF-B4GALNT2) and the predominantly expressed protein was found to be the short isoform [8].

Most of the Golgi glycosyltransferases share a common topology and domain structure in eukaryotic cells: they are type II transmembrane proteins exhibiting a short CT, a unique transmembrane domain, a stem and a catalytic domain located within the Golgi lumen [9]. It has long been appreciated that correct final glycosylation depends on correct localization and organization of glycosyltransferases within the Golgi apparatus [10–12]. Although extensively studied, molecular mechanisms orchestrating spatial and functional organization of Golgi glycosyltransferases remain poorly understood. It is currently accepted that the N-terminal region encompassing the CT, the transmembrane, and the stem domains is responsible for their appropriate Golgi retention [13–15] although this region represents a highly divergent domain of glycosyltransferases across vertebrate evolution [16]. A few studies have reported a potential role of glycosyltransferase CT for their specific localization to the Golgi [17–21], intracellular trafficking dynamics [22], or to atypical cellular localization [23].

Using confocal fluorescence microscopy approaches, we examined the subcellular distribution of each of the two B4GALNT2 protein isoforms in stably transfected LS174T colonic cells established previously [24] and observed distinct distribution of the two isoforms. To tackle this issue, we followed the expression of fluorescent protein (eGFP/mCy)-tagged isoforms of the B4GALNT2 in transiently transfected HeLa cells, which are cells commonly used in studies to map Golgi enzymes distribution [25]. We report here a similar subcellular localization of the two B4GALNT2 isoforms into the Golgi cisternae and most intriguingly, an unusual subcellular distribution of the LF-B4GALNT2 isoform localizing to vesicle-like structures by virtue of its extended CT. Molecular deletion analysis conducted as a first step to decipher the mechanism by which the LF-B4GALNT2 is targeted to these vesicles indicated that it is signal mediated. Our study points to the existence of a dibasic signal essential for ER exit and of a crucial and dominant signal for post-Golgi targeting present within the first 22 amino acid residues of the LF-B4GALNT2 CT.

Results

Differential B4GALNT2 isoforms localization and trafficking in LS174T colonic cells

We previously reported that the human *B4GALNT2* gene produces two protein isoforms with the same catalytic domain, one of which shows an unusual extended CT of 66 amino acid residues [7,8]. As an initial step to assess the subcellular distribution of the two B4GALNT2 protein isoforms, we used confocal microscopy and an anti-B4GALNT2 polyclonal antibody directed against a common domain of the stem region in the stably transfected colon cancer LS174T cells, expressing either the short isoform (LS174T-S2) or the long isoform (LS174T-L21) previously established by Malagolini *et al.* [24]. We previously noticed that each stably transfected cell line drives the expression of similar levels of the two B4GALNT2 isoform, although the LS174T-S2 produce higher levels of Sd^a

antigen on glycoproteins compared to the LS174T-L21 [8], which could be partly due to the previously documented higher enzymatic activity of the short isoform [24]. We show here that the two isoforms localized to a Golgi-like perinuclear region in LS174T-S2 and LS174T-L21 cells and partially colocalized with GM130, a widely used *Cis*-Golgi marker [26], whereas no B4GALNT2 isoform could be detected in the LS174T-mock cells (Fig. 1A). Interestingly, in addition to this Golgi-like distribution, we observed also an unusual punctuated cytoplasmic distribution in LS174T-L21 suggesting the existence of an additional localization of this long isoform (Fig. 1A). Similar distribution of the LF-B4GALNT2 was observed in the LS174T-L20 cell line (data not shown) expressing lower levels of the long isoform [24]. To check the enzymatic activity of both B4GALNT2 isoforms, we also analyzed the production of Sd^a antigen in LS174T-S2 and LS174T-L21 cells using the anti-Sd^a monoclonal antibody KM694. Completely absent in the LS174T-mock cells, Sd^a synthesis is observed for both B4GALNT2 isoforms, although it appears to be

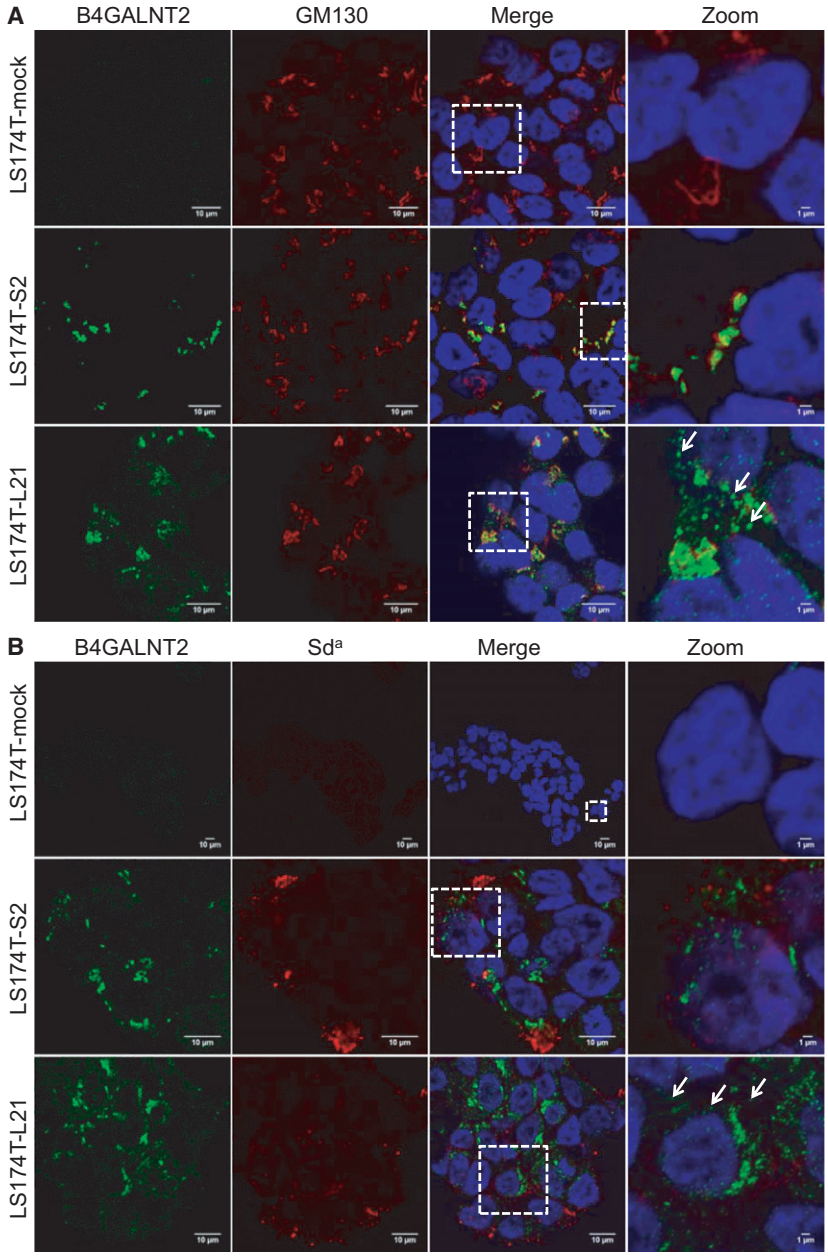

Fig. 1. Localization of the two B4GALNT2 protein isoforms and Sd^a in stably transfected colon cancer LS174T cells. (A) LS174T-S2, LS174T-L21, and LS174T-mock cells [24] were fixed and labeled with rabbit anti-B4GALNT2 antibody (green). Mouse anti-GM130 antibody was used to mark the Golgi complex (red). Cells were counterstained with Alexa 488-labeled goat anti-(rabbit IgG) and Alexa 568-labeled goat anti-(mouse IgG). Coverslips were analyzed by confocal fluorescence microscopy. DAPI was used for nuclei staining (blue). Merged images are shown and areas of overlapping distribution in the same optical section appear as yellow. Zoomed pictures are shown and white arrows highlight the punctate distribution of LF-B4GALNT2 (green) only observed in LS174T-L21 cells. (B) LS174T-S2, LS174T-L21, and LS174T-mock cells were fixed and labeled with rabbit anti-B4GALNT2 antibody (green). The mouse anti-Sd^a antibody KM694 was used to visualize the activity of B4GALNT2 (i.e., Sd^a antigen) in the different cells (red). Cells were counterstained with Alexa 488-labeled goat anti-(rabbit IgG) and Alexa 568-labeled goat anti-(mouse IgM) antibodies. Coverslips were analyzed by confocal fluorescence microscopy. DAPI was used for nuclei staining (blue). Merged and zoomed images are shown and areas of overlapping distributions in the same optical section appear as yellow. White arrows highlight the punctate distribution of LF-B4GALNT2 (green) in LS174T-L21 cells. Images in both panels are representative of two independent experiments. Scale bars: 10 μm (zoom: 1 μm).

less abundant in LS174T-L21 cells than in LS174T-S2 (Fig. 1B), as previously reported [8,24].

We also conducted antibody uptake experiments to assess the possible intracellular traffic of the B4GALNT2 isoforms in LS174T cells. Both types of stably transfected LS174T cells were incubated at 37 °C for 3 h with the anti-B4GALNT2 antibody. Cells were then washed, fixed, and permeabilized. Antibody tracking in the various LS174T cells using confocal microscopy and an anti-rabbit IgG Alexa 488 staining showed no anti-B4GALNT2 antibody staining in LS174T-S2, whereas anti-B4GALNT2 antibody staining could be detected in LS174T-L21 (Fig. 2A). Furthermore, we observed strong colocalization at the LS174T-L21 cell surface of the LF-B4GALNT2 with the B4GALNT2 product Sd^a (Zoom/Merge in Fig. 2A). We confirmed transient cell surface exposure of the LF-B4GALNT2 performing cell surface biotinylation. Biotin-labeled cell surface proteins were affinity purified with streptavidin and run on SDS/PAGE. Western blotting carried out with the anti-B4GALNT2 indicated the presence of a faint band of the expected molecular weight for the LS174T-L21 cells, whereas no band could be detected in the LS174T-S2 and LS174T-mock cells (Fig. 2B). Altogether, these observations further suggest an exposure of the LF-B4GALNT2 at the cell surface, whereas the SF-B4GALNT2 is retained in the Golgi apparatus.

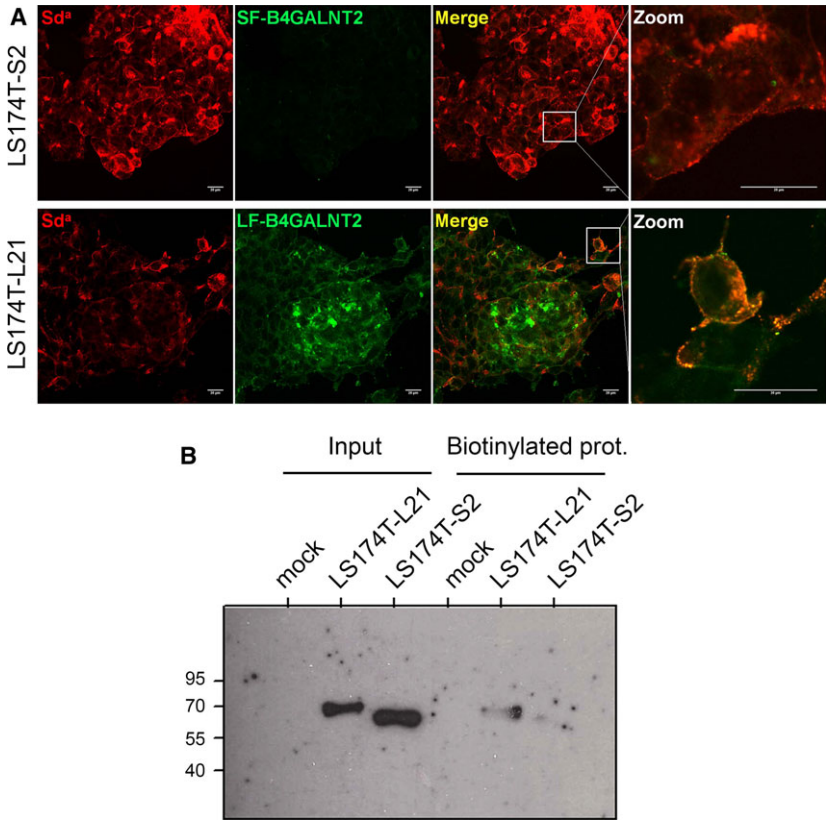

Fig. 2. Trafficking of the two B4GALNT2 isoforms in stably transfected colon cancer LS174T cells. (A) Anti-B4GALNT2 antibody uptake in LS174T-S2, LS174T-L21, and LS174T-Mock. LS174T-S2, LS174T-L21, and LS174T-mock were grown on coverslips and incubated 3 h with the anti-B4GALNT2 antibody, fixed and processed for immunofluorescence using Alexa 488-labeled goat anti-(rabbit IgG) antibody (green). In parallel, staining of the Sd^a antigen was performed as a control, using anti-Sd^a antibody KM694, followed by Alexa 568-labeled goat anti-(mouse IgM) antibody (red). No staining for the anti-B4GALNT2 antibody could be observed in LS174T-S2, whereas LS174T-L21 exhibited vesicular and plasma membrane staining. Coverslips were analyzed by confocal fluorescence microscopy using the inverted Leica SP5. Scale bars: 20 μm. (B) Cell surface biotinylation experiments in LS174T-S2, LS174T-L21, and LS174T-mock. Seventy percent confluent LS174T-mock, LS174T-S2 and LS174T-L21 cells were incubated 3 h at 37°C to allow subcellular trafficking and potential transient exposure of the B4GALNT2 isoforms at the cell surface. Cell surface biotinylation was achieved using Sulfo-NHS-SS-Biotin as described in material and methods. One milligram of extracted proteins was incubated overnight at 4°C with Streptavidin beads and purified proteins were run on 8% SDS/PAGE. Total B4GALNT2 (input) and cell surface B4GALNT2 (biotinylated proteins) was visualized by western blotting using the anti-B4GALNT2 antibody. No staining for B4GALNT2 was observed in the biotinylated fraction obtained from LS174T-S2, whereas the long B4GALNT2 isoform was detected in the biotinylated fraction obtained from LS174T-L21

Table 1. Primers and plasmids list used for B4GALNT2 constructions. Name of the construct, sequence of the primer and name of the expression vectors used are indicated in this Table. Restriction sites are underlined in the primer sequence and cutting sites of type IIs restriction enzymes are indicated in bold.

Construct	PCR	Forward primer	Reverse primer	Vector
SF-B4GALNT2		CCTAGCTAGCGCCACCATGACTTCGGGCGGCTCG	GAAGATCTCTGCGGCACATTGGAGATG	pfx
LF-B4GALNT2		CCTAGCTAGCGCCACCATGGGGAGCGCTGGCTTTT	CGGGATCCCCTGCGGCACATTGGAGATG	pmCherry-N1
ST3GAL4		AGGAATTCCTGCTGCCTGCTGGCCACCATGGTCAG	CAGCTCTTGCGGATCCCCGAAGGACGTGAGG	mCherry
LF-Δ139-566		CCTAGCTAGCGCCACCATGGGGAGCGCTGGCTTTT	TTCAGGATCCCACTGATTTTTCGGGAACAGCC	pmCherry-N1
SF-Δ79-506		CCTAGCTAGCGCCACCATGACTTCGGGCGGCTCG	TTCAGGATCCCACTGATTTTTCGGGAACAGCC	peGFP-N1
LF-Δ2-22	PCR1	GCCCGCCTGGCATTTATGC	TTTGGTCTCC**CCAT**GGTGGCGCTAGCGGATCTGAC	pmCherry-N1
	PCR2	TTTGGTCTCC**ATGG**TCTCGGGGACGCCCGAGTGTGGGA	GCTTCTGGCTGTCATCAGCCAC	
LF-Δ23-43	PCR1	GCCCGCCTGGCATTTATGC	TTTGGTCTCC**ACAT**CCCGGCCGCGAGAGGCCAC	pmCherry-N1
	PCR2	TTTGGTCTCC**ATGT**GAACTCAGAGGCGCTGACCCAGCCTG	GCTTCTGGCTGTCATCAGCCAC	
LF-Δ44-64	PCR1	GCCCGCCTGGCATTTATGC	TTTGGTCTCC**CAAG**CAGAGAGCCCCGAAG	pmCherry-N1
	PCR2	TTTGGTCTCC**CTTG**GGCTCGAGATTTCTGTGGCTCCTC	GCTTCTGGCTGTCATCAGCCAC	
LF-Δ23-64	PCR1	GCCCGCCTGGCATTTATGC	TTTGGTCTCC**ACAT**CCCGGCCGCGAGAGGCCAC	pmCherry-N1
	PCR2	TTTGGTCTCC**ATGT**GGCTCGAGATTTCTGTGGCTCCTC	GCTTCTGGCTGTCATCAGCCAC	
LF-Δ2-8	PCR1	GCCCGCCTGGCATTTATGC	TTTGGTCTCC**CCAT**GGTGGCGCTAGCGGATCTGAC	pmCherry-N1
	PCR2	TTTGGTCTCC**ATGG**GAAAATTCCACGTGGAAGTGG	GCTTCTGGCTGTCATCAGCCAC	
LF-Δ9-15	PCR1	GCCCGCCTGGCATTTATGC	TTTGGTCTCC**GCCA**CGGAAAAGCCAGCGCTCC	pmCherry-N1
	PCR2	TTTGGTCTCC**TGGC**CTCTCGCGGCCGGGAATGTG	GCTTCTGGCTGTCATCAGCCAC	
LF-Δ16-22	PCR1	GCCCGCCTGGCATTTATGC	TTTGGTCTCC**ACCA**CTTCCACGTGGAATTTTCCCAC	pmCherry-N1
	PCR2	TTTGGTCTCC**TGGT**CTCGGGGACGCCCGAGTGTG	GCTTCTGGCTGTCATCAGCCAC	
CT-B4GALNT2-ST3GAL4	PCR1	AACTGCCCACTTGGCAGTACATC	TTTGGTCTCG**AGCG**AGCCCTGACGGCGGCTCCTC	pmCherry-N1
	PCR2	TTTGGTCTCG**CGCT**CCTGGCCATGTTGGCTCTGGTC	GGGTCGAAGTGGGCAGATTCAG	

The FEBS Journal **285** (2018) 3442–3463 © 2018 The Authors. *The FEBS Journal* published by John Wiley & Sons Ltd on behalf of Federation of European Biochemical Societies.

B4GALNT2-tagged isoforms localization in HeLa cells

To define more precisely the differential subcellular localization of the two B4GALNT2 isoforms, DNA constructs were made for the production of full-length B4GALNT2 C-terminal tagged fluorescent proteins (Table 1). The SF-B4GALNT2 was coupled with green fluorescent protein (eGFP), whereas the LF-B4GALNT2 was linked to red fluorescent protein (mCy) (Fig. 3A). HeLa cells previously shown to be devoid of B4GALNT2 [8], were chosen for transient transfection of the various B4GALNT2 constructs and confocal microscopy observations. Each tagged full-length B4GALNT2 isoform was individually transfected in HeLa cells. As observed in LS174T cells, a compact perinuclear Golgi-like distribution of both isoforms was observed and the LF-B4GALNT2 showed an additional atypical punctate distribution suggesting vesicle-like structures (White arrows in Fig. 3B). Cotransfection of the two tagged B4GALNT2 isoforms in HeLa cells showed an almost perfect overlap in the Golgi complex and the presence of additional red vesicles widely distributed in the cytoplasm containing the LF-B4GALNT2 (Fig. 3C). We also aimed to give a more quantitative evaluation of the atypical distribution of the LF-B4GALNT2 since the Golgi morphology of LF-B4GALNT2-transfected cells could appear slightly fragmented [27]. Toward this aim, we counted the total number of red or green vesicles distinct from the Golgi region per cell from LF-B4GALNT2- and SF-B4GALNT2-transfected cells from several independent experiments and plotted in whiskers plot (Fig. 3D), as described in the material and methods section. Further statistical analysis revealed a highly significant ($P < 0.001$) difference of vesicles number in the LF-B4GALNT2- and SF-B4GALNT2-transfected cells (Fig. 3D).

To assess intracellular trafficking of both B4GALNT2 isoforms, HeLa cells transiently cotransfected with LF-B4GALNT2-mCy and SF-B4GALNT2-eGFP were monitored by confocal video microscopy (Videos S1 and S2). Our data highlighted very distinct recorded vesicle numbers (on average, 62 vesicles per LF-B4GALNT2-transfected cell and 0.5 vesicles per SF-B4GALNT2-transfected cell) and remarkable motilities of the LF-B4GALNT2-mCy vesicles with an average track length of 9 μm ±8.8 and velocity of 4.1 $\mu m \cdot s^{-1}$. An example of the trajectories of these vesicles, with apparently high mobility back and forth from the *trans*-Golgi toward the periphery of the cell, is illustrated in Fig. 4.

Fine subcellular localization of both B4GALNT2 isoforms in transfected HeLa cells

To gain insight into SF-B4GALNT2 and LF-B4GALNT2 fine Golgi localization and into the nature of the vesicles containing LF-B4GALNT2, we conducted colocalization of confocal microscopy experiments in transiently transfected HeLa cells using well-described markers of the secretory pathway. Firstly, we showed that the tagged full-length SF-B4GALNT2 and LF-B4GALNT2 did not colocalize with the endoplasmic reticulum marker calnexin (Figs 5 and 6) nor did the red LF-B4GALNT2 vesicles colocalize with the ER–Golgi intermediate compartment (ERGIC) marker ERGIC-53 (data not shown). We then used giantin, a *cis*/*medial*-Golgi marker localized to tubular cisternal Golgi elements potentially representing fenestrated connections between cisternal stacks [28]. As observed previously with GM130 in LS174T cells, both SF-B4GALNT2 and LF-B4GALNT2 exhibited a low degree of colocalization with giantin further suggesting a late Golgi localization of the two isoforms. We observed partial overlap (yellow arrows) of the tagged SF-B4GALNT2 and LF-B4GALNT2 with the *trans*-Golgi marker B4GALT1 and the *trans*-Golgi network markers TGN46 and TMEM165, a recently described cation transporter [29]. Besides its *trans*-Golgi localization and compared to the SF-B4GALNT2, the LF-B4GALNT2 showed an obvious and distinct vesicle-like pattern (white arrows in Fig. 6) that we aimed to further characterize. We detected no colocalization of the LF-B4GALNT2-containing vesicles with the endosomal marker Rab11A (data not shown) and very partial overlap with the early endosomal antigen-1 marker (EEA1) and the lysosome-associated membrane protein 2 marker (LAMP2) (yellow arrows, Fig. 6) as assessed by analysis of the distribution of fluorescence in vesicles using the RGB profiler plugin (ImageJ), whereas no colocalization could be detected for the SF-B4GALNT2 (Fig. 5). Altogether, these data suggested that besides its predominant Golgi localization, the LF-B4GALNT2 isoform also exhibits an atypical subcellular localization to vesicles mostly distinct from Golgi apparatus, endosomal, or lysosomal compartments.

The extended cytoplasmic tail of the LF-B4GALNT2 isoform contains Golgi/vesicle-targeting signals

We next wanted to gain insight into the mechanisms involved into the vesicles targeting of the LF-B4GALNT2. Since the presence of the extended CT is

Fig. 3. Localization of the two fluorescently tagged full-length B4GALNT2 isoforms in transfected HeLa cells. (A) Schematic of the SF-B4GALNT2-eGFP and LF-B4GALNT2-mCy reporter constructs. The full-length SF-B4GALNT2 (506 amino acids) was tagged with eGFP and the full length LF-B4GALNT2 (566 amino acids) was tagged with mCherry (mCy). Cytoplasmic (C), transmembrane (TM), and luminal catalytic domains are represented giving a sense of the topology of the enzyme in the Golgi apparatus. The numbers indicate amino acids of the CT, TM, stem, and catalytic domain of each B4GALNT2 isoform. (B) Individual transfections in HeLa cells. Each tagged full-length B4GALNT2 isoform (SF-B4GALNT2-eGFP and LF-B4GALNT2-mCy) was transfected individually in HeLa cells. Analysis of their subcellular localization by confocal microscopy as described in material and methods showed a Golgi-like distribution. Besides the compact perinuclear localization of both isoforms, the LF-B4GALNT2 showed an atypical punctate distribution as underlined by white arrows. Images are representative of two independent experiments. Scale bars: 10 μm. (C) Cotranfections. Cotransfection of the two tagged B4GALNT2 isoforms (SF-B4GALNT2-eGFP and LF-B4GALNT2-mCy) in HeLa cells showed overlap in the Golgi area, and the presence of additional red vesicle-like structures indicated by white arrows that contain the LF-B4GALNT2. Images are representative of two independent experiments. Scale bars: 10 μm. (D) Quantitative assessment of the vesicles. The total number of red or green vesicles distinct from the Golgi region was counted per cell line from 19 LF-B4GALNT2 and 17 SF-B4GALNT2 transfected HeLa cells from two independent experiments. The ICY software (http://icy.bioimageanalysis.org) was used for vesicle quantitation. Numbers of vesicles were plotted in whiskers plots where means and SEMs are depicted and statistical analysis using ANOVA test (Kruskal–Wallis nonparametric test with selected comparison using Dunn's post hoc test (GRAPPAD PRISM 5.0 software) revealed a highly significant (***: $P < 0.001$) difference of vesicles number in FL-B4GALNT2-mCy and SF-B4GALNT2-eGFP transfected cells (GRAPPAD PRISM 5.0 software).

the only structural difference between the two isoforms, we used two fluorescent truncated B4GALNT2 proteins, with their entire common catalytic domain deleted, but containing their respective CT (LF-Δ139-566-B4GALNT2-mCy and SF-Δ79-506-B4GALNT 2-eGFP, Fig. 7A), and studied their subcellular localization. HeLa cells were first transiently transfected with each truncated protein. Figure 7B shows essentially the same subcellular distribution as described for the full-length B4GALNT2 isoforms, in the Golgi apparatus for both isoforms and in vesicles for the LF-B4GALNT2 (white arrows). Similarly, cotransfection of the two tagged LF-Δ139-566-B4GALNT2 and SF-Δ79-506-B4GALNT2 isoforms showed an almost perfect overlap in the Golgi complex and the presence of additional red vesicles containing the LF-B4GALNT2 (Fig. 7C).

Next, we conducted colocalization confocal microscopy experiments in transiently transfected HeLa cells using markers of the secretory pathway, that is, calnexin, giantin, TMEM165, EEA1, and LAMP2. As previously described for the full-length, tagged B4GALNT2 isoforms, the truncated isoforms showed predominantly Golgi localization and the LF-Δ139-566-B4GALNT2 showed an additional vesicular distribution distinct from Golgi, endosomes, or lysosomes (Fig. 8A,B). Taken together, these data strongly suggested a critical role of the CT of the LF-B4GALNT2 for targeting this isoform in intracellular vesicles.

Mechanistic insights into the role of the cytoplasmic tail of LF-B4GALNT2

To tackle this issue, we made additional constructs using the full-length cDNA of the human α2,3-sialyltransferase-IV (*ST3GAL4*) obtained previously [30] fused with eGFP (ST3GAL4-eGFP) or with the mCherry (ST3GAL4-mCy) protein at the C terminus as illustrated in Fig. 9A (Table 1). Each construct transiently transfected in HeLa cells had the expected Golgi distribution and did not display any vesicle staining (data not shown). Another construct was made fusing the first 66 amino acid residues of the CT of the LF-B4GALNT2 to the ST3GAL4 deleted of its first eight amino acids leading to the chimeric protein CT-B4GALNT2-ST3GAL4-mCy (Fig. 9A). The ST3GAL4-eGFP and CT-B4GALNT2-ST3GAL4-mCy were cotransfected in HeLa cells. Confocal microscopy analysis not only indicated a Golgi-like colocalization of the two chimeric proteins but also an additional vesicular distribution of the CT-B4GALNT2-ST3GAL4-mCy (Fig. 9B). These data demonstrated the critical role played by the extended CT sequence on the observed post-Golgi localization of the LF-B4GALNT2 and strongly suggested the presence of a molecular signal embedded in the extended CT.

To determine which region of the CT could be implicated and refine the amino acid sequence signal, four deletion mutants of the full-length LF-B4GALNT2 coupled wiht mCherry at the C terminus were constructed that were devoid of the first 2–22, or 23–43, or 44–64 or 23–64 amino acid residues (LF-Δ2-22, LF-Δ23-43, LF-Δ44-64, LF-Δ23-64, Fig. 10A) (Table 1). These constructs were then transiently transfected in HeLa cells and their subcellular localization examined using confocal fluorescence microscopy. As shown in Fig. 10B, the subcellular localization of the LF-Δ23-43, LF-Δ44-64, LF-Δ23-64 constructs is similar to the one observed for the full length LF-B4GALNT2 (Fig. 6). Remarkably, the LF-Δ2-22 construct showed a diffuse distribution within the cell

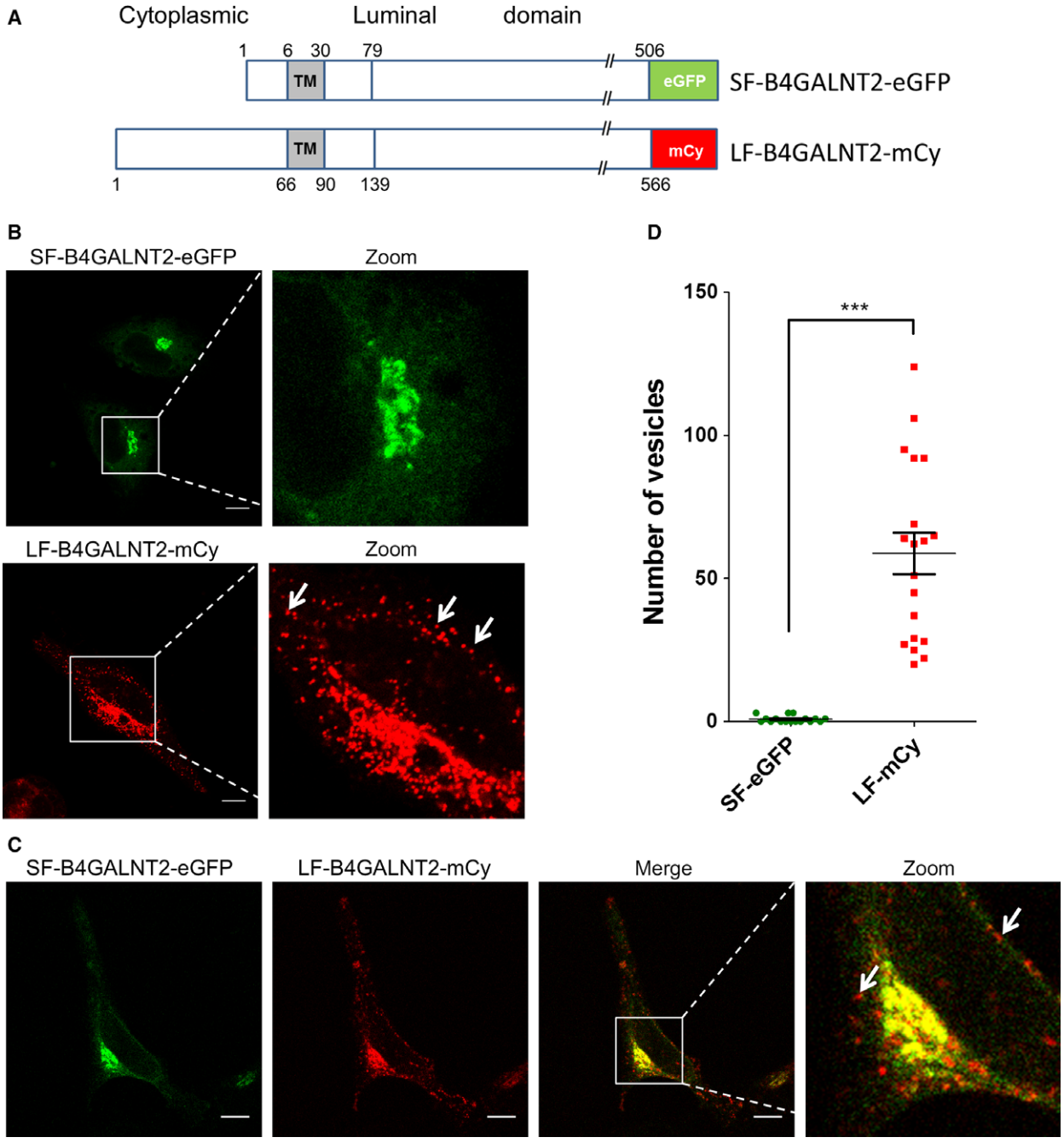

indicating that this 2–22 region is essential for Golgi and post-Golgi targeting. Furthermore, we carried out quantitation of the red vesicles distribution in each series of transfected cells and observed a slight and not significant decrease in the number of vesicles in the LF-Δ23-43-, LF-Δ44-64-, LF-Δ23-64-B4GALNT2-transfected cells, whereas it was significantly ($P < 0.001$) decreased in the LF-Δ2-22-B4GALNT2-transfected cells (Fig. 10C).

In an attempt to distinguish the ER-export signal from the vesicle-targeting signal of the LF-B4GALNT2, we further dissected this amino acid sequence contained within amino acids 2–22. Three additional constructs were made using the full-length LF-B4GALNT2-mCy, with deletion of the first 2–8, 9–15 or 16–22 amino acid residues (LF-Δ2-8, LF-Δ9-15, LF-Δ16-22 depicted in Fig. 11A). After transfection in HeLa cells, immunofluorescence assays using

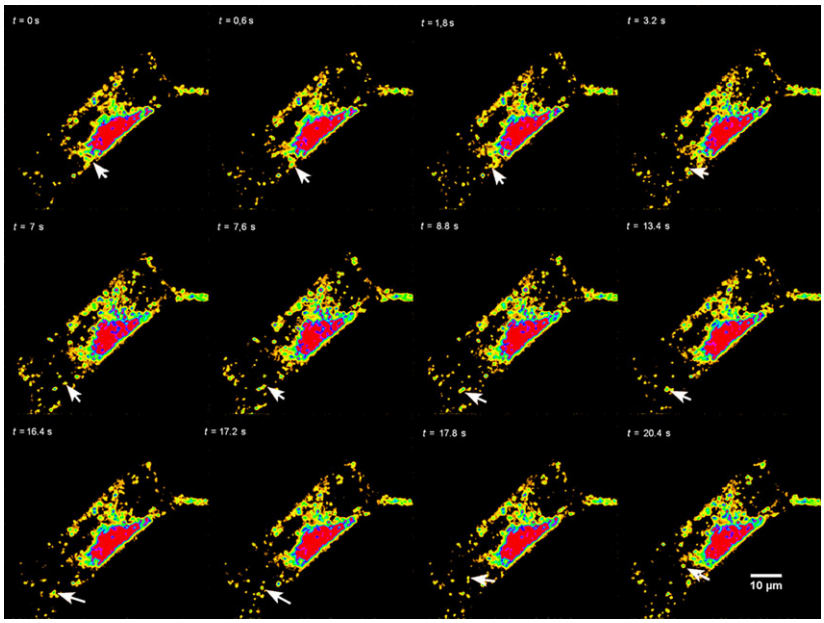

Fig. 4. Live cell trafficking of LF-B4GALNT2-mCy in transiently transfected HeLa cells. Transiently cotransfected HeLa cells with LF-B4GALNT2-mCy and SF-B4GALNT2-eGFP were monitored by confocal video-microscopy (spinning-disk confocal). To illustrate the complex LF-B4GALNT2 trajectories, this figure shows 12 images extracted at several times from the Video S1, between $t = 0$ s and $t = 20.4$ s. The arrow indicates the same vesicle over time in each image. This vesicle leaves the *trans*-Golgi and goes toward the periphery of the cell, takes contact with other immobile vesicles. This vesicle comes back toward the *trans*-Golgi, but does not merge. The speed of displacement of this vesicle is nonconstant (~ 2.8 µm·s^{-1}). The images were viewed using a thermo look-up table (LUT) highlighting vesicles without specific thresholding.

either the ER marker anti-calnexin or the *trans*-Golgi marker anti-TMEM165 demonstrated the Golgi and vesicle localization (white arrows) of the LF-Δ2-8 and LF-Δ16-22 constructs, whereas a perfect colocalization of LF-Δ2-22 was observed with the ER marker (Fig. 11B). However, the LF-Δ9-15 construct localized to the Golgi compartment and showed no vesicular distribution compared to the other constructs (Fig. 11B). The total number of vesicles was counted per cell from LF-Δ2-8-, LF-Δ9-15-, and LF-Δ16-22-B4GALNT2-mCy-transfected cells and plotted in whiskers plots and statistical analyses revealed a highly significant ($P < 0.001$) reduction in vesicles number in the LF-Δ9-15–B4GALNT2-mCy-transfected cells (Fig. 11C).

Altogether, these data demonstrated that the first 22 amino acids of the CT are crucial for both ER exit and post-Golgi subcellular localization. More interestingly, our results highlight the importance of the 9-15 heptapeptide (GKFHVEV) of the B4GALNT2 CT as a vesicular targeting signal.

Discussion

We have shown previously that the human *B4GALNT2* gene is expressed primarily in the healthy digestive tract and drives the expression of two major transcripts encoding two protein isoforms, the so-called short and long B4GALNT2 isoforms responsible for the synthesis of Sd^a/Cad antigen [1,6–8]. Preliminary human evolutionary genomics analysis indicated the occurrence of a human-specific genetic change in the *B4GALNT2* gene that gave rise to the long transcript variant as a result of the use of a new alternative first exon. The very unusual feature of the resulting long B4GALNT2 protein isoform is its

Fig. 5. Intracellular colocalization of full-length SF-B4GALNT2-eGFP with subcellular markers calnexin, giantin, TGN46, TMEM165, B4GALT1, EEA1, and LAMP2, in transiently transfected HeLa cells. Subcellular localization of short B4GALNT2 isoform (green) was examined and compared to the pattern of the different markers (red) by confocal microscopy. SF-B4GALNT2-eGFP mostly colocalized with *trans*-Golgi markers. Right panels show the intensity profiles of SF-B4GALNT2 (green) and of the each marker (red) in selected vesicles using the RGB profiler plugin (Image J). Images are representative of two independent experiments. Scale bars: 10 µm.

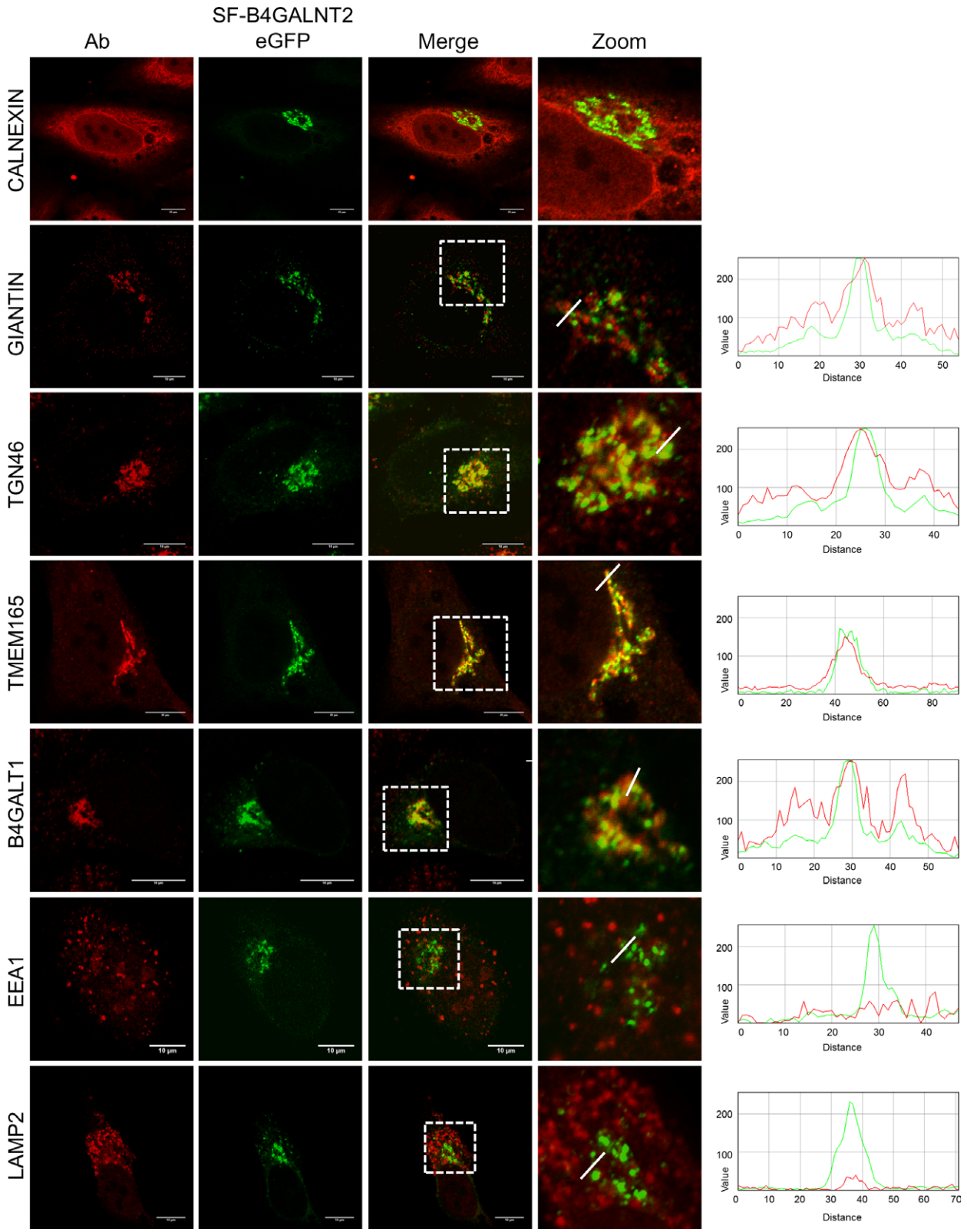
SF-B4GALNT2
Ab
eGFP
Merge
Zoom
CALNEXIN
GIANTIN
TGN46
TMEM165
B4GALT1
EEA1
LAMP2
10 µm
Value
Distance

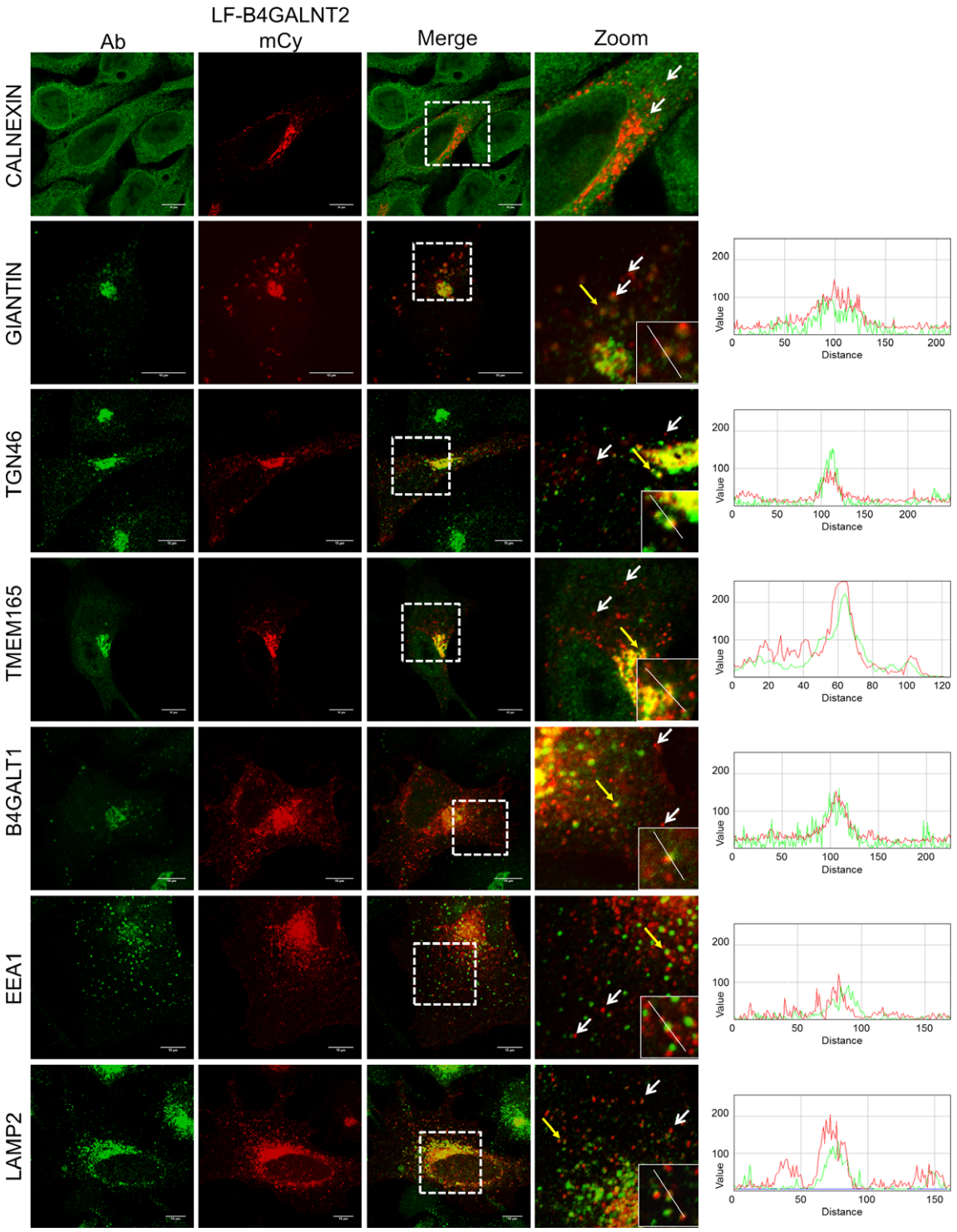

Fig. 6. Intracellular colocalization of full length LF-B4GALNT2-mCy with subcellular markers calnexin, giantin, TGN46, TMEM165, B4GALT1, EEA1, and LAMP2 in transiently transfected HeLa cells. Subcellular localization of the long B4GALNT2 isoform (red) was examined and compared to the pattern of the different markers (green) by confocal microscopy. LF-B4GALNT2-mCy mostly colocalized with *trans*-Golgi markers and showed a vesicle-like distribution indicated by white arrows in the zoomed picture. In addition, LF-B4GALNT2-mCy showed also a very partial overlap with the different TGN/endosomal/lysosomal markers used (yellow arrows). Right panels show the intensity profiles of LF-B4GALNT2 (red) and of the each marker (green) in selected vesicles using the RGB profiler plugin (Image J). Images are representative of two independent experiments. Scale bars: 10 μm.

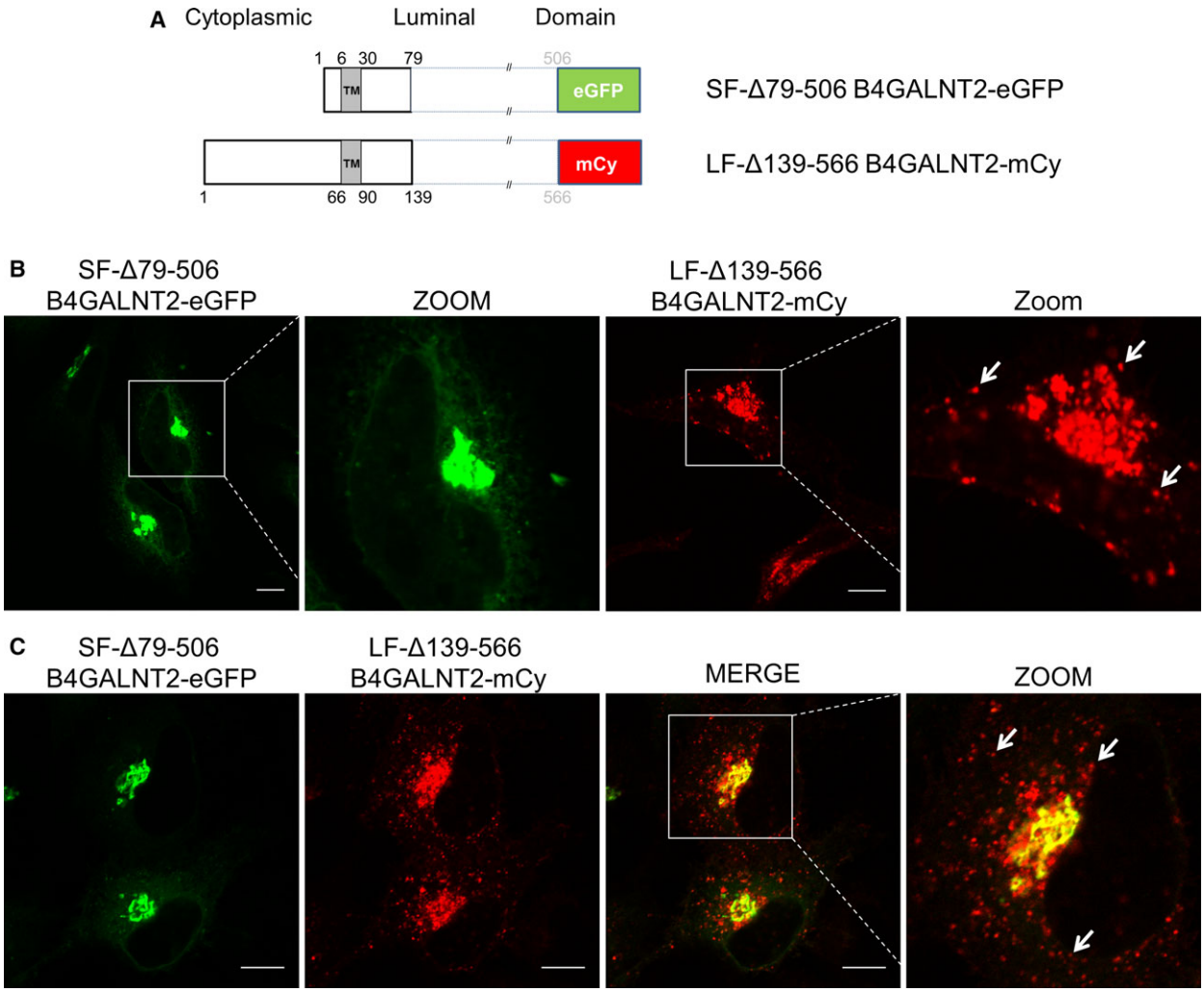

Fig. 7. Localization of the two fluorescently tagged truncated B4GALNT2 isoforms in transfected HeLa cells. (A) Schematic of the truncated SF-B4GALNT2-eGFP and LF-B4GALNT2-mCy reporter constructs. The SF-Δ79-506-B4GALNT2 (79 amino acids) was tagged with eGFP and the LF-Δ139-566-B4GALNT2 (139 amino acids) was tagged with mCherry (mCy). The numbers indicate amino acids of the cytoplasmic, transmembrane, and stem domains (black numbers) and of the deleted catalytic domain (gray numbers) of each B4GALNT2 isoform. (B) Individual transfections. Each tagged truncated B4GALNT2 isoform deleted of the catalytic domain (SF-Δ79-506-B4GALNT2-eGFP and LF-Δ139-566-B4GALNT2-mCy) was transfected individually in HeLa cells. Analysis of their subcellular localization by confocal microscopy showed a Golgi-like distribution. Besides the compact perinuclear localization of both isoforms, the LF-Δ139-566-B4GALNT2 showed an atypical punctate distribution as described for the full-length LF-B4GALNT2 as underlined by white arrows in the zoomed picture. (C) Cotranfections of the two tagged truncated B4GALNT2 isoforms (SF-Δ79-506-B4GALNT2-eGFP and LF-Δ139-566-B4GALNT2-mCy) in HeLa cells showed overlap in the Golgi area, and the presence of additional red vesicle-like structures that contain the LF-B4GALNT2 indicated by white arrows in the zoomed picture. Images are representative of two independent experiments. Scale bars: 10 μm.

extraordinarily long CT of 66 amino acid residues, whereas the short B4GALNT2 isoform presents a six-amino acid CT comparable to that of the previously described mouse ortholog [31]. The transmembrane and catalytic domains remain identical for the two isoforms. Using confocal fluorescence microscopy approaches, we examined the subcellular distribution of the two B4GALNT2 isoforms in the stably transfected LS174T [24] and of eGFP/mCherry-tagged isoforms of B4GALNT2 in transiently transfected HeLa cells. This analysis of the subcellular localization demonstrated a similar subcellular distribution of the two isoforms in the Golgi apparatus. The two B4GALNT2 isoforms are found across the *trans*-Golgi cisternae of the Golgi apparatus to the TGN (Figs 5 and 6), similarly to the previously described late acting

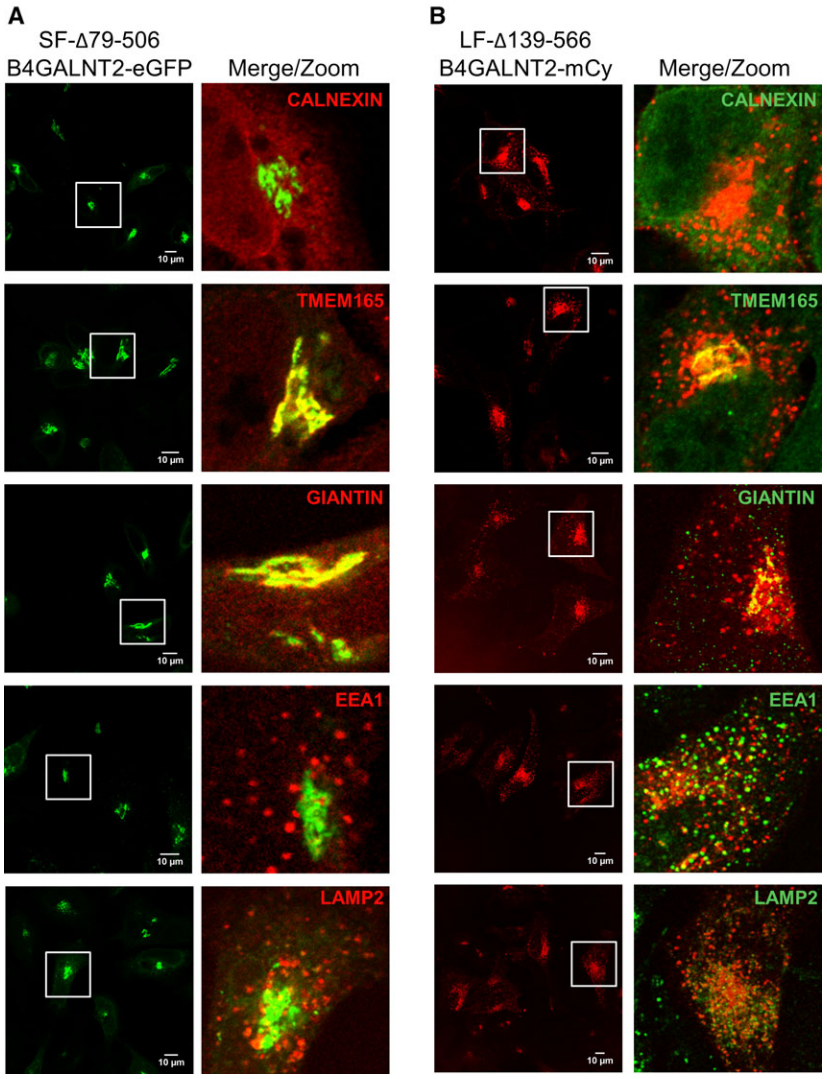

Fig. 8. Subcellular localization and colocalization of the two B4GALNT2 isoforms deleted of their catalytic domain using immunofluorescence. Constructions of the short and long B4GALNT2 isoforms deleted of the catalytic domain, that is, SF-Δ79-506-B4GALNT2 and LF-Δ139-566-B4GALNT2 were tagged with eGFP or mCy at the C terminus, respectively. Intracellular colocalization studies of SF-Δ79-506-B4GALNT2 (A) and LF-Δ139-566-B4GALNT2 (B) with subcellular markers calnexin, giantin, TGN46, TMEM165, B4GALT1, EEA1, LAMP2 were conducted in transiently transfected HeLa cells. Zoomed pictures of the merged images: SF-Δ79-506-B4GALNT2-eGFP (green)/marker (red) (A), and LF-Δ139-566-B4GALNT2-mCy (red)/marker (green) (B), are presented. Images are representative of two independent experiments. Scale bars: 10 µm.

B4GALT1 and ST6Gal I enzymes [32,33]. Intriguingly, in addition to this Golgi distribution, the long isoform localizes to vesicles distributed in the cytoplasm.

The eukaryotic glycosyltransferases located in the Golgi are type II proteins with a usually short cytoplasmic (C) tail, a unique transmembrane (T) domain, a stem (S) region highly variable in length, and a large catalytic domain oriented within the Golgi lumen. To date, molecular mechanisms and signals underpinning the subcellular distribution and Golgi compartmentalization of glycosyltransferases appear to be multifactorial and are still poorly understood [12,34,35]. As reviewed previously [36], numerous studies have highlighted the crucial role of the CTS domain for the correct orchestration of Golgi glycosylation steps. In the nineties, two models have been proposed to explain Golgi localization and retention of glycosyltransferases, although none of them is entirely satisfactory: (a) the lipid bilayer thickness model depending on the length and hydrophobicity of the

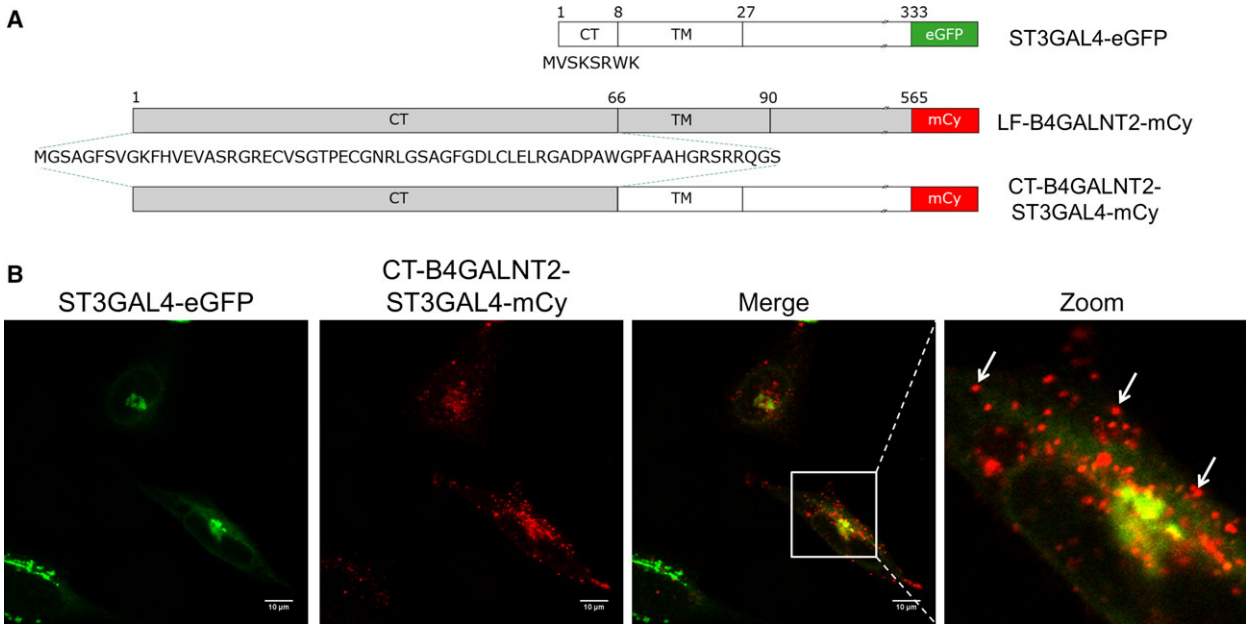

Fig. 9. Fluorescence microscopy with chimeric ST3GAL4/CT-B4GALNT2. (A) Schematic illustration of various constructs. Constructs were made with mCherry at the C terminus of the full-length B4GALNT2 (LF-B4GALNT2-mCy) and of the B4GALNT2 cytoplasmic tail/CT-deleted ST3GAL4 (CT-B4GALNT2-ST3GAL4-mCy) chimeric protein and eGFP was added at the C terminus of the full-length ST3GAL4 (ST3GAL4-eGFP). (B) Distribution of chimeric constructs within transfected HeLa cells. Fluorescently tagged constructs ST3GAL4-eGFP and CT-B4GALNT2-ST3GAL4-mCy were transiently cotransfected in HeLa cells. Subcellular localization of the various isoforms was examined by confocal microscopy. White arrows in the zoomed image indicate the vesicle distribution of the chimeric CT-B4GALNT2-ST3GAL4-mCy construct. Images are representative of two independent experiments. Scale bars: 10 μm.

transmembrane domain and the thickness of the Golgi membrane [37,38] and (b) the oligomerization or kin recognition model that assumes the formation of glycosyltransferase homo- or hetero-oligomers through disulfide bridges when they reach the correct Golgi compartment [39,40]. Our data in Fig. 7, using both B4GALNT2 isoforms deleted of their entire catalytic domain (SF Δ79-506-eGFP and LF Δ139-566-mCy) clearly indicate that the catalytic domain is not an important parameter for the Golgi localization of the two B4GALNT2 isoforms, as previously reported for the bovine B4GALT1 [41]. These observations are consistent with a model in which the bilayer thickness plays a major role. However, hydropathy analysis of the human B4GALNT2 potential membrane spanning region and conservation analysis reveals that this 23-amino acid hydrophobic domain is not highly conserved in other B4GALNT2 orthologs (data not shown). This sequence heterogeneity further suggests that physical properties like length and hydrophobicity and/or additional features functioning in a combinatorial manner could be involved in the *trans*-Golgi targeting of the two human isoforms. Interestingly, our data shown in Figs 10 and 11 evidenced the existence of additional strong signals in the long B4GALNT2 isoform CT, since deletion of the first 2–22 amino acid residues abrogates Golgi targeting. Similar observations have been made in the past that the CT of the Golgi resident enzymes α1,3-galactosyltransferase and α1,2-fucosyltransferase could be sufficient to confer their specific Golgi localization [17,18].

Our confocal microscopy studies conducted with cells expressing each B4GALNT2 isoform and transiently transfected cells provided compelling evidences of an atypical subcellular localization of the long B4GALNT2 isoform. Beside its expected *trans*-Golgi and TGN targeting, the long isoform localizes in a vesicle population distinct from Golgi, endosomal, or lysosomal compartments that was not reported previously for a glycosyltransferase (Fig. 6). Such an unusual cellular localization of glycosyltransferases at post-Golgi sites including the plasma membrane has been rarely described before and remains a controversial issue. A few examples include the β1,4-galactosyltransferase 1 (B4GALT1), which also exists in short and long isoforms diverging in their N-terminal region with a cell surface expression and no vesicles localization [42,43], an α1,2-fucosyltransferase (FUT1) [23]

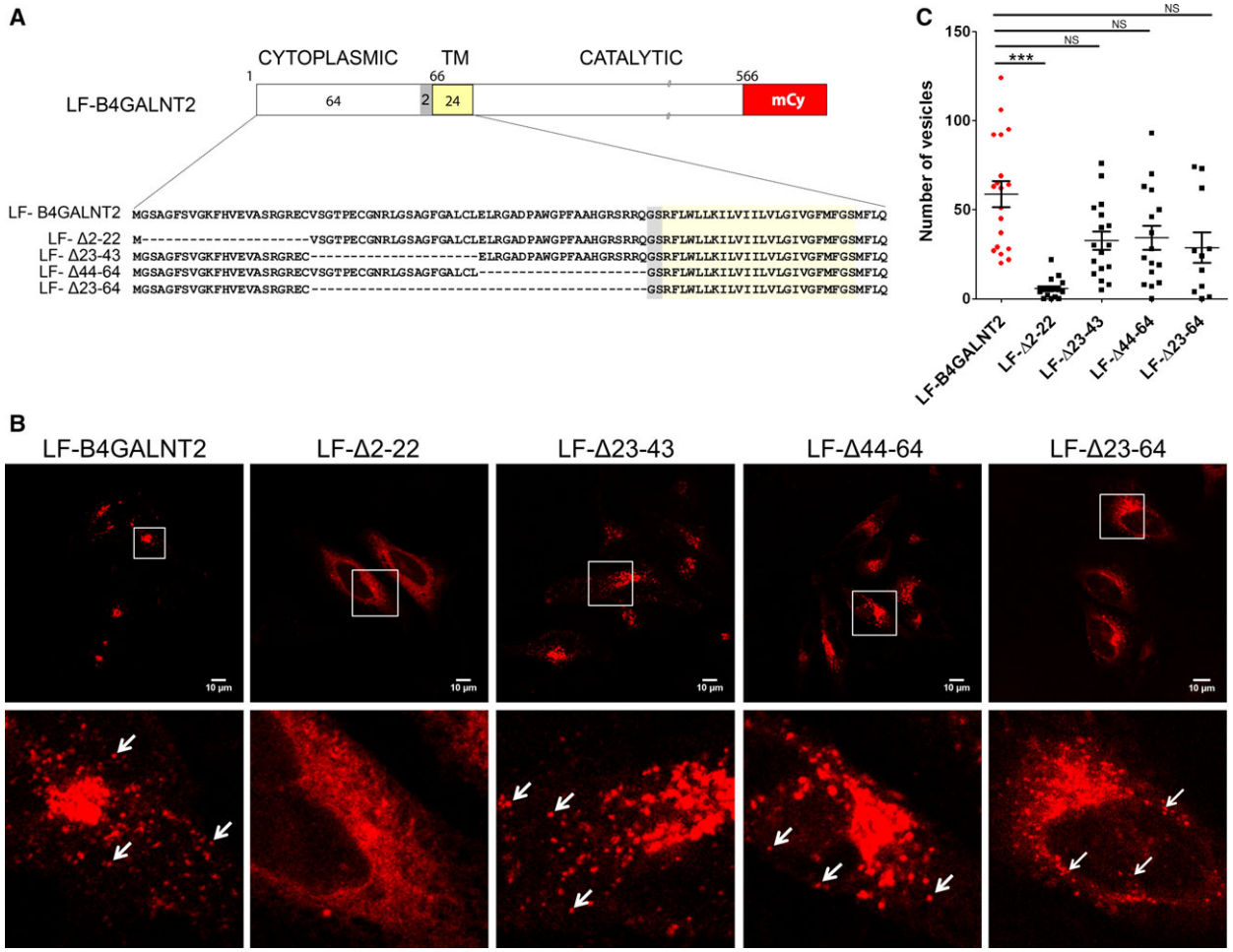

Fig. 10. Fluorescence microscopy with large deletion mutants of the long B4GALNT2 cytoplasmic tail. (A) Schematic illustration of various cytoplasmic tail deletion mutants. Chimeric constructs were made with mCherry (mCy) at the C terminus of the full-length B4GALNT2. LF-B4GALNT2 was deleted of the first third of its cytoplasmic tail (LF-Δ2-22), or second third (LF-Δ23-43), or of the third third (LF-Δ44-64), or of the two last thirds of its cytoplasmic tail (LF-Δ23-64). (B) Subcellular localization of cytoplasmic tail deletion mutants of the long B4GALNT2 isoform. Fluorescently tagged deletion constructs of the long B4GALNT2-mCy isoform LF-Δ2-22, LF-Δ23-43, LF-Δ44-64, and LF-Δ23-64 were transiently expressed in HeLa cells. Subcellular localization of the various isoforms was examined by confocal microscopy. A zoom is inserted where white arrows indicate the vesicle distribution of the construct. Images are representative of three independent experiments. Scale bars: 10 µm. (C) Quantification of vesicles in Hela cells transiently transfected with the cytoplasmic tail deletion mutants (LF-Δ2-22, LF-Δ23-43, LF-Δ44-64, and LF-Δ23-64) of the long B4GALNT2 isoform. The total number of red vesicles distinct from the Golgi region was counted per cell from 19 LF-B4GALNT2-mCy cells, 17 FL-Δ2-22-B4GALNT2-mCy cells, 17 FL-Δ23-43-B4GALNT2-mCy cells, 16 FL-Δ44-64-B4GALNT2-mCy cells, and in 11 FL-Δ23-64-B4GALNT2-mCy cells from two independent experiments. The ICY software (http://icy.bioimagea nalysis.org) was used for vesicle quantitation. The number of vesicles was plotted in whiskers plots where means and SEMs are depicted. No significant variations (ns) in the number of vesicles was observed for the various mutants, except the FL-Δ2-22-B4GALNT2-mCy mutant ($P < 0.001$), as assessed by the Kruskal–Wallis nonparametric test with selected comparison using Dunn's post hoc test (GRAPPAD PRISM 5.0 software).

and an α1,3-fucosyltransferase (FUT6) localizing in Weibel–Palade bodies of human endothelial cells [44]. In this study, we also examined the dynamic intracellular transport of both B4GALNT2 isoforms using video-microscopy (Videos S1 and S2). The trajectory of the same vesicle containing LF-B4GALNT2 was followed overtime in living cells and indicated that this vesicle originated from the Golgi apparatus, went toward the periphery of the cell and came very close to another immobile vesicle (Fig. 4). This vesicle appeared to come back toward the Golgi apparatus, but did not merge further, supporting previous observations made in LS174T-L21. Our data also demonstrated specific kinetics and fate for the LF-

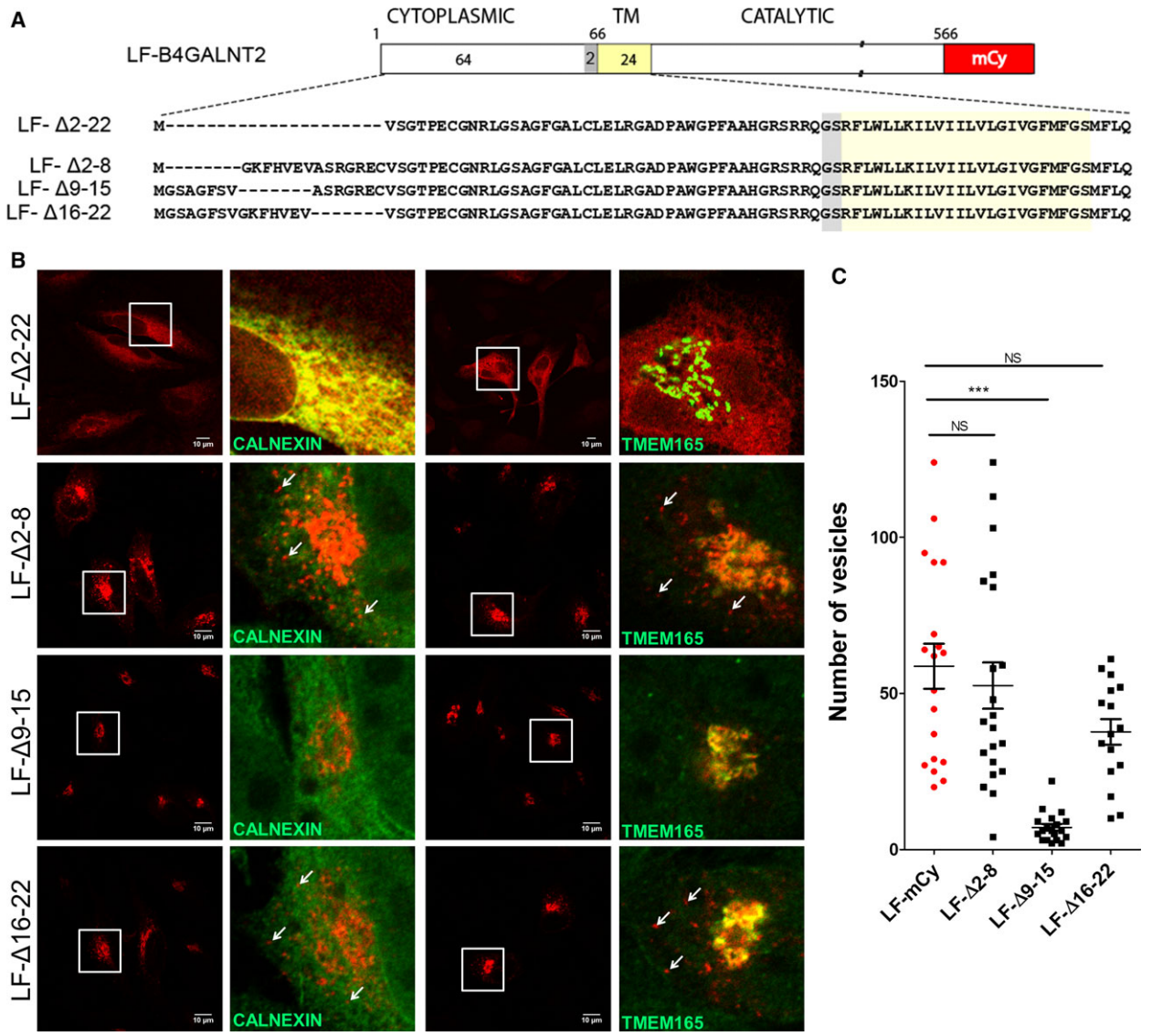

Fig. 11. Fluorescence microscopy with small deletion mutants in the 2–22 region of the long B4GALNT2 cytoplasmic tail. (A) Schematic illustration of various cytoplasmic tail deletion mutants. Three additional constructs deleted in the 2–22 region of the LF-Δ2-22 (full-length C-terminal mCy-tagged B4GALNT2 deleted of the first third of its cytoplasmic tail) were made: the LF-Δ2-8, LF-Δ9-15, and the LF-Δ16-22. (B) Subcellular localization of cytoplasmic tail deletion mutants of the long B4GALNT2 isoform. Fluorescent tagged deletion constructs of the long B4GALNT2-mCy isoform, that is, LF-Δ2-22, LF-Δ2-8, LF-Δ9-15, and LF-Δ16-22 were transiently expressed in HeLa cells and immunolocalized by confocal microscopy. Cells were colabeled with anti-TMEM165 (*trans*-Golgi marker, red) or with anti-calnexin antibody (ER marker, green), and zoomed merged images are presented. Images are representative of two independent experiments. Scale bars: 10 μm. (C) Quantification of vesicles in Hela cells transiently transfected with the cytoplasmic tail deletion mutants LF-Δ2-22, LF-Δ2-8, LF-Δ9-15, and LF-Δ16-22 of the long B4GALNT2-mCy isoform. The total number of red vesicles distinct from the Golgi region was counted per cell from 21 FL-Δ2-8-B4GALNT2-mCy cells, 19 FL-Δ9-15-B4GALNT2-mCy cells, and 16 FL-Δ16-22-B4GALNT2-mCy cells from two independent experiments. The ICY software (http://icy.bioimageanalysis.org) was used for vesicles quantitation. The number of vesicles were plotted in whiskers plots where means and SEMs are depicted. No significant variations (ns) in the number of vesicles was observed for the various mutants, except the FL-Δ9-15-B4GALNT2-mCy mutant ($P < 0.001$), as assessed by the Kruskal–Wallis nonparametric test with selected comparison using Dunn's post hoc test (GRAPPAD PRISM 5.0 software).

B4GALNT2 isoform containing vesicles indicating that their trafficking within the cell is not the result of simple bulk flow of Golgi-derived vesicles to the cell surface. Furthermore, antibody uptake experiment evidenced a particular traffic of the long isoform with transient exposure at the cell surface strongly

suggesting that the long isoform follows a novel Golgi to plasma membrane transport pathway in living cells. Biotinylation of cell surface proteins and subsequent WB analysis of streptavidin purified proteins corroborated these findings. Indeed, to our knowledge, this is the first report of a post-Golgi localization of terminal glycosyltransferase in dynamic vesicles. In the light of these data, it is tempting to speculate that the long B4GALNT2 isoform could be implicated in the trafficking of cell surface proteins and plays a determinant role in the regulation of terminal glycosylation steps, which remains to be established.

Our study provides also essential mechanistic insights into the targeting process of the long B4GALNT2 isoform to the *trans*-Golgi and post-Golgi vesicles. While the CTS domain of most glycosyltransferases (including SF-B4GALNT2) is sufficient for their Golgi targeting, our deletion studies in the CT of the LF-B4GALNT2 isoform indicate the presence in the 2–22 region of strong and critical signals that are determinant for Golgi and vesicles localization (Figs 10 and 11), although no binding motif for adaptor proteins could be detected [45]. Deletion of the 23–64 region of the CT does not perturb the Golgi/vesicles targeting indicating low impact of other requirements such as context or distance from the TM. However, further dissection of the amino acid sequence contained within the 2–22 peptide of the LF-B4GALNT2 CT lead us to distinguish the ER-export signal from the vesicle targeting signal. Previous studies have reported the existence of a dibasic motif [K/R] X [K/R] in the CT of some Golgi glycosyltransferases that facilitates ER exit to Golgi through direct interaction with the small GTPase Sar1 [46–49]. Interestingly, we noted the presence of an RGR motif at positions 18–20 in the LF-B4GALNT2 CT that is absent in the LF-Δ2-22-B4GALNT2, which could explain ER retention of this construct. Furthermore, we highlighted the existence of a major signal at position 9–15 in the CT of the LF-B4GALNT2 that is critical for vesicles targeting and post-Golgi trafficking. This signal is strong enough to override the absence of the ER exit signal in the LF-Δ16-22-B4GALNT2 and directs this construct to the Golgi and post-Golgi compartments. In summary, we describe in this study an unusual post-Golgi targeting of a human Golgi glycosyltransferase and determine the essential signals involved. This further suggests additional function (s) of the LF-B4GALNT2 and likely another level of regulation of Sd^a/Cad expression in human tissues that remains to be determined.

Materials and methods

Plasmids of human long and short B4GALNT2 isoforms for the expression of chimeric fluorescent proteins

Full-length B4GALNT2 constructs (GenBank accession numbers AJ517770 and AJ517771) were obtained in our laboratory from plasmids described previously [7]. The GFP expression vector pFx was a kind gift of Dr Jack Röhrer (University of Zürich) and expression vectors pEGFP-N1 and pmCherry-N1 were from Clontech. For GFP fusion, full-length or truncated SF-B4GALNT2 PCR products were amplified using oligonucleotide primers containing *Nhe*I-*Bgl*II restriction sites for directed ligation in *Nhe*I-*Bgl*II digested pFx vector (Table 1). Similarly, for mCherry and GFP fusions, full-length or truncated LF-B4GALNT2 were constructed using PCR in pmCherry-N1 or pEGFP-N1 vectors using *Nhe*I-*BamH*I restriction sites (Table 1). To obtain all the combination of fusion constructs, SF and LF exchange fragments were carried out using *Nhe*I and the internal B4GALNT2 *BspE*I restriction sites [located at 1078 bp in AJ517770 (LF) and at 860 bp in AJ517771 (SF)]. Full-length cDNA of the human α2,3-sialyltransferase-IV (*ST3GAL4*) was obtained previously [30] and fused with eGFP (ST3GAL4-eGFP) or mCherry (ST3GAL4-mCy) sequence. Deletion mutations Δ2–22, Δ23–43, Δ44–64, Δ23–64, Δ2–8, Δ9–15, and Δ16–22 were introduced in the CT of the pmCherry-LF-B4GALNT2 plasmid using two PCR reactions with primer pairs containing a *Bsa*I site and PCR products (PCR1 and PCR2 in Table 1) were recombined by *Bsa*I digestion/Ligation. Finally, each fragment was digested with *Nhe*I and *BsmB*I and the wild-type *Nhe*I- *BsmB*I fragment in pmCherry-LF-B4GALNT2 was exchanged with the deleted *Nhe*I-*BsmB*I fragment. The *BsmB*I restriction site is located at 426 bp in AJ517770 (LF-B4GALNT2) and at 208 bp in AJ517771 (SF-B4GALNT2). To construct fusion of the first 66 amino acid residues of the CT of the LF-B4GALNT2 (CT-B4GALNT2) to the ST3GAL4 deleted of its first eight amino acids leading to the chimeric protein CT-B4GALNT2-ST3GAL4-mCy, a similar strategy of deletion mutation construction was used (PCR1 and PCR2 joined by *Bsa*1/ligation reaction (Table 1), the exchanged fragment in pmCherry-ST3GAL4 was *NdeI-BsmBI*. All constructions were entirely sequenced (GATC Biotech, Konstanz, Germany).

Cell culture, transfections and western blotting

Cell lines were from ATCC (LGC Standards SARL, Molsheim, France), and stably transfected LS174T (LS174T-S2 expressing the short B4GALNT2 isoform, LS174T-L21 expressing the long B4GALNT2 isoform, LS174T-mock

transfected with empty pcDNA3 vector) were previously described [24]. Human colon carcinoma cells LS174T were cultured in Eagle's minimal essential medium (EMEM) with 2 mM L-glutamine supplemented with 10% or 20% FBS. HeLa cells were cultured in Dulbecco's modified eagle's medium (DMEM) supplemented with 10% FBS (Life technologies, Carlsbad, CA, USA) and 20 mM L-glutamine. The cells were maintained at 37 °C under humid atmosphere and 5% CO_2.

HeLa cells grown on Petri dishes were transiently transfected with the different constructs (Table 1) using Lipofectamine 2000 (Thermo Fisher Scientific Bioscience, Villebon-sur-Yvette, France). We set up transfection conditions using various amount of plasmids ranging from 0.5 to 5 μg and finally choose to use the lowest amount of plasmid as possible (i.e., 0.5 μg). Proteins extraction from LS174T-mock cells, LS174T-S2, LS174T-L21, or transiently transfected HeLa cells was achieved as previously described [8]. Protein concentration was determined with the Micro BCA Protein Assay Reagent kit (Biorad, Marnes-la-coquette, France). Four to 25 μg of total protein extract were boiled for 5 min in Laemmli sample buffer with 2.5% β-2-mercaptoethanol (Sigma Aldrich, Saint Louis, MO, USA) and resolved by 8% SDS/PAGE. Proteins were transferred onto a nitrocellulose membrane (200 mA, 2 h). Detection of B4GALNT2 was achieved with anti-B4GALNT2 (rabbit polyclonal antibody, Cat. HPA015721-100μl, lot#A74836, Sigma Aldrich) as already described [8].

Indirect Immunofluorescences and antibodies

Twenty-four hours after seeding on glass coverslips, HeLa cells were transiently transfected with the different constructs (Table 1) using Lipofectamine 2000 (Thermo Fisher Scientific Bioscience). Similarly, LS174T-S2, LS174T-L21, and LS174T-mock cells were grown on glass coverslips, fixed and processed for fluorescence microscopy. Twenty-four hours after transfection, cells were washed twice with PBS, fixed either with 4% paraformaldehyde (PAF) in PBS for 20 min at room temperature (RT) or with ice cold methanol for 10 min. Coverslips were washed three times with PBS. After a permeabilization step of 30 min at RT in PBS containing 0.5% of Triton X100, cells were washed two times with PBS and incubated in blocking solution (PBS containing 0.2% (w/v) BSA) during 1 h. Cells were incubated overnight at 4 °C in humid chambers with primary antibodies diluted in blocking solution. After three washing steps, cells were incubated 1 h in dark at RT with secondary antibodies diluted in blocking solution. Finally, cells were washed three times in PBS and coverslips were mounted using Dako fluorescent mounting medium for observation using fluorescent confocal microscopy.

For immunofluorescence assays, primary antibodies anti-B4GALT1 (mAb GT2/36/118, Enzo Life Sciences, Villeurbanne, France), anti-TGN46 (rabbit pAb, Cat AHP1586, lot#170114, Biorad AbD serotech GmbH, Bio-Rad AbD Serotec Ltd., Oxon, UK), anti-EEA1 (mAb Cat. 610456, lot#4087703, Becton Dickinson, Le Pont-de-Claix, France), anti-LAMP2 (mAb, cat. Sc-18822, clone H4B4, lot#C2613, Santa Cruz Biotechnologies Inc., Heidelberg, Germany), anti-TMEM165 (pAb, Cat. HPA038299, lot#A78664, Sigma Aldrich), anti-GM130 (mAb, Cat. 610822, lot#5072921, Becton Dickinson), anti-Rab11 (rabbit mAb clone 3H18L5, 700184, lot #756772B, Thermo Fisher Scientific Bioscience), and anti-ERGIC-53 (mouse mAb, ref ALX-804-602-C100, clone G1/93, Enzo-lot : L26372) were diluted at 1/100[e], anti-giantin (rabbit pAb, Cat PRB144C, Covance, Rueil-Malmaison, France) was diluted at 1/150[e] and anti-calnexin (pAb, Cat. ADI-SPA-860-F, lot#12301304, ENZO Life Sciences) was diluted at 1/250[e]. Secondary antibodies, Alexafluor® 488 and Alexafluor® 568 anti-mouse or -rabbit IgG (H+L) were from Life Technologies/Molecular Probes and diluted at 1/600[e] in blocking buffer. After three washing with PBS, coverslips were mounted on glass slides with Mowiol.

Confocal microscopy, quantitation and trajectories of vesicles analyses

Sublocalization's studies of the fluorescent proteins and immunostaining were achieved either with an inverted Leica SP5 (Mannheim, Germany), or an inverted Zeiss LSM780 (Oberkochen, Germany) or an inverted Zeiss LSM700 confocal microscope with a 40× or 63× oil immersion objectives. The eGFP protein and the Alexafluor® 488 were visualized using the argon laser with an excitation at 488 nm and an emission range between 500 and 560 nm. The red fluorophores were visualized using the supercontinuum laser source (NKT, Cologne, Germany) with two different settings, the mCherry was excited at 590 nm and the Alexafluor® 568 was excited at 568 nm, the emission ranges were respectively between 610–700 nm and 578–700 nm. Data were collected using LAS AF LITE software (Leica) or using ZEN PRO 2.1 software (Zeiss) and analyzed with FIJI-WIN32 [50] and ICY FREE software.

For quantitation of vesicles, the ICY software (http://icy.bioimageanalysis.org) was used. First, the entire cells were individually delimited by drawing polygonal area and masking the perinuclear Golgi region (Golgi and Golgi-associated vesicles defined by colocalization data) by regions of interest (ROIs) to keep only the region of interest containing distinct vesicles. Then, the vesicles per cell were detected using the plugin 'spot detector' with three scales to determine the spot's size and the sensitivity of detection for each size: scale 2 corresponding to an object size of 3 pixels at 25% of sensitivity, scale 3 (7 pixels) at 90%, and scale 4 (13 pixels) at 90% of sensitivity. Parameters of ROIs detection were adapted to the stably transfected LS174T cells (LS174T-L21) and to the transiently transfected HeLa cells. For these latter, 10–20 cells were counted to establish the average number of vesicles per cell

and for each construct. Since no Golgi compartment could be detected in the FL-Δ2-22-B4GALNT2-mCy transfected HeLa cells (Figs 9 and 10), we considered the whole cell for vesicle counting. Data were plotted as whiskers plots and statistical analyses were performed using GRAPHPAD PRISM 5.0 software, GraphPad Software Inc., La Jolla, CA, USA) and were compared using a nonparametric Kruskal–Wallis test followed by Dunn's comparison post-test. Values were considered significantly different (*) with $P < 0.05$ (***: $P < 0.001$). The ICY software with spot detector and spottracking modules (A. Dufour, Institut Pasteur Paris) was used for the analysis of LF-B4GALNT2 vesicles trajectories.

Antibody uptake and cell surface biotinylation experiments

LS174T-mock cells, LS174T-S2 and LS174T-L21 cells were grown until 70% of confluence on glass coverslips and washed four times with PBS. Cells were incubated for 3 h at 37 °C with 20 $\mu g \cdot mL^{-1}$ anti-B4GALNT2 antibody or control anti-HA antibody in medium containing 10 $\mu g \cdot mL^{-1}$ leupeptin. Cells were washed five times with ice-cold PBS, and fixed with ice-cold methanol for 10 min. Cells on coverslips were then incubated overnight at 4 °C in humid chambers with anti-Sd^a primary antibody diluted 1 : 500 in blocking solution. Coverslips were then washed three times with PBS and labeled at RT in dark for 1 h with Alexafluor® 488-conjugated goat anti-(rabbit IgG) and Alexafluor® 568-conjugated goat anti-(mouse IgM) antibody diluted 1 : 600 in blocking solution. After three washings with PBS, coverslips were mounted on glass slides with Mowiol, and both B4GALNT2 antibody signal and Sd^a antigen expression were studied by confocal microscopy.

Seventy % confluent LS174T-mock cells, LS174T-S2 and LS174T-L21 cells were plated and washed four times with Dulbecco PBS (DPBS, pH8). Biotinylation was achieved essentially as described before [51] using Sulfo-NHS-SS-Biotin (Biotin: EZ link, Life Technologies). Cells were incubated 3 h at 37 °C to allow subcellular trafficking and potential transient exposure of the B4GALNT2 isoforms at the cell surface and then washed three times in DPBS. One milligram of extracted proteins was incubated overnight at 4 °C with streptavidin beads (EMD Milipore Corp, Billerica, MA, USA). Purified proteins were run on 8% SDS/PAGE as mentioned above.

Video-microscopy and dynamics analyses

Confocal acquisitions were performed with spinning-disk confocal system (Yokogawa CSU-X1, Tokyo, Japan) adapted on a Leica DMI6000B inverted microscope with diode laser source emitting at a wavelength of 488 nm and 514 nm and EM-CCD camera (Li^2CAM MD) with pixel size of 10.3 μm^2. Cells were imaged using a 63X oil immersion objective (Leica HCX Plan Apo NA 1.4). Emitted fluorescence was then successively routed by a dichroic mirror (Semrock Di01-T405/488/568/647) and spectrally filtered (Chroma, HQ545/306). Final size of pixel image 0.21 μm x 0.21 μm was obtained. We have made acquisitions for transfected cells either with LF-B4GALNT2-mCy or with two transfections, SF-B4GALNT2-eGFP and LF-B4GALNT2-mCy. The time acquisition per image was 25 ms. Stacks of four optical sections, with 100 ms by stack were made. For acquisition with two channels, we alternated the stack by channel. Videos are constituted by 601 images for a total of 30 seconds.

Acknowledgements

This work was supported partly by the Centre National de La Recherche Scientifique (CNRS), by the University of Lille1, by the ANR-2010-BLAN-120401 grant (project Galfish, to AH-L, LH) and ANR-15-CE14-0001-01 (project SOLV-CDG to FF) from the Agence Nationale de la Recherche (ANR), by the Région Nord-Pas de Calais (program Arcir dynamique to AH-L, LH), by the Ligue régionale de la recherche contre le cancer (to AH-L), by the University of Bologna (to FD) and from Pallotti Legacy for Cancer Research (to FD). The authors acknowledge the BioImaging Center of Lille (BICeL) for confocal imaging. The anti-Sd^a antibody KM694 was a generous gift from the Pharmaceutical research center, Kyowa Hakko Kogyo Co. Ltd. (Tokyo, Japan). The authors are very grateful to L. Danglot (INSERM U894, 'Membrane traffic in Health and Disease', Paris) for helping with the vesicles trajectories analyses with Icy.

Conflict of interests

The authors declare that they have no competing interests.

Author contributions

SGD, FF, LH, FD, and AHL conceived and designed the experiments. CS, VC, and FD made constructs for molecular biology. MM, DV, SGD, LP, MN, and CS performed cell culture and transfections experiments. CS, SGD, DV, AG, AS, and FF used confocal microscopy and FF supervised subcellular localization experiments. MG, MH, CS, and LH used confocal laser scanning microscope. SGD, VC, FF, LH, and AHL drafted the manuscript and all the authors approved the final manuscript.

References

1 Dall'Olio F, Malagolini N, Chiricolo M, Trinchera M & Harduin-Lepers A (2014) The expanding roles of the Sd(a)/Cad carbohydrate antigen and its cognate glycosyltransferase B4GALNT2. *Biochim Biophys Acta* **1840**, 443–453.

2 Dohi T, Ohta S, Hanai N, Yamaguchi K & Oshima M (1990) Sialylpentaosylceramide detected with anti-GM2 monoclonal antibody. Structural characterization and complementary expression with GM2 in gastric cancer and normal gastric mucosa. *J Biol Chem* **265**, 7880–7885.

3 Morton JA, Pickles MM & Vanhegan RI (1988) The Sda antigen in the human kidney and colon. *Immunol Invest* **17**, 217–224.

4 Dohi T, Hanai N, Yamaguchi K & Oshima M (1991) Localization of UDP-GalNAc:NeuAc alpha 2,3Gal-R beta 1,4(GalNAc to Gal)N-acetylgalactosaminy ltransferase in human stomach. Enzymatic synthesis of a fundic gland-specific ganglioside and GM2. *J Biol Chem* **266**, 24038–24043.

5 Malagolini N, Dall'Olio F, Di Stefano G, Minni F, Marrano D & Serafini-Cessi F (1989) Expression of UDP-GalNAc:NeuAc alpha 2,3Gal beta-R beta 1,4 (GalNAc to Gal) N-acetylgalactosaminyltransferase involved in the synthesis of Sda antigen in human large intestine and colorectal carcinomas. *Cancer Res* **49**, 6466–6470.

6 Lo Presti L, Cabuy E, Chiricolo M & Dall'Olio F (2003) Molecular cloning of the human beta1,4 N-acetylgalactosaminyltransferase responsible for the biosynthesis of the Sd(a) histo-blood group antigen: the sequence predicts a very long cytoplasmic domain. *J Biochem* **134**, 675–682.

7 Montiel MD, Krzewinski-Recchi MA, Delannoy P & Harduin-Lepers A (2003) Molecular cloning, gene organization and expression of the human UDP-GalNAc:Neu5Acalpha2-3Galbeta-R beta1,4-N-acetylgalactosaminyltransferase responsible for the biosynthesis of the blood group Sda/Cad antigen: evidence for an unusual extended cytoplasmic domain. *Biochem J* **373**, 369–379.

8 Groux-Degroote S, Wavelet C, Krzewinski-Recchi M, Portier L, Mortuaire M, Mihalache A, Trinchera M, Delannoy P, Malagolini N, Chiricolo M *et al.* (2014) B4GALNT2 gene expression controls the biosynthesis of Sda and sialyl Lewis X antigens in healthy and cancer human gastrointestinal tract. *Int J Biochem Cell Biol* **53**, 442–449.

9 Colley KJ, Lee EU, Adler B, Browne JK & Paulson JC (1989) Conversion of a Golgi apparatus sialyltransferase to a secretory protein by replacement of the NH2-terminal signal anchor with a signal peptide. *J Biol Chem* **264**, 17619–17622.

10 Gill DJ, Tham KM, Chia J, Wang SC, Steentoft C, Clausen H, Bard-Chapeau EA & Bard FA (2013) Initiation of GalNAc-type O-glycosylation in the endoplasmic reticulum promotes cancer cell invasiveness. *Proc Natl Acad Sci USA* **110**, E3152–E3161.

11 Nilsson T, Au CE & Bergeron JJ (2009) Sorting out glycosylation enzymes in the Golgi apparatus. *FEBS Lett* **583**, 3764–3769.

12 Opat AS, van Vliet C & Gleeson PA (2001) Trafficking and localisation of resident Golgi glycosylation enzymes. *Biochimie* **83**, 763–773.

13 Colley KJ, Lee EU & Paulson JC (1992) The signal anchor and stem regions of the beta-galactoside alpha 2,6-sialyltransferase may each act to localize the enzyme to the Golgi apparatus. *J Biol Chem* **267**, 7784–7793.

14 Fenteany FH & Colley KJ (2005) Multiple signals are required for alpha2,6-sialyltransferase (ST6Gal I) oligomerization and Golgi localization. *J Biol Chem* **280**, 5423–5429.

15 Uliana AS, Giraudo CG & Maccioni HJ (2006) Cytoplasmic tails of SialT2 and GalNAcT impose their respective proximal and distal Golgi localization. *Traffic* **7**, 604–612.

16 Harduin-Lepers A (2013) Vertebrate sialyltransferases. In *Sialobiology: Structure, Biosynthesis and Function Sialic acid glycoconjugates in health and diseases* (Tiralongo J & Martinez-Duncker I, eds), pp. 139–187. Bentham Science, United Arab Emirates.

17 Milland J, Russell SM, Dodson HC, McKenzie IF & Sandrin MS (2002) The cytoplasmic tail of alpha 1,3-galactosyltransferase inhibits Golgi localization of the full-length enzyme. *J Biol Chem* **277**, 10374–10378.

18 Milland J, Taylor SG, Dodson HC, McKenzie IF & Sandrin MS (2001) The cytoplasmic tail of alpha 1,2-fucosyltransferase contains a sequence for golgi localization. *J Biol Chem* **276**, 12012–12018.

19 Sousa VL, Brito C & Costa J (2004) Deletion of the cytoplasmic domain of human alpha3/4 fucosyltransferase III causes the shift of the enzyme to early Golgi compartments. *Biochim Biophys Acta* **1675**, 95–104.

20 de Graffenried CL & Bertozzi CR (2004) The roles of enzyme localisation and complex formation in glycan assembly within the Golgi apparatus. *Curr Opin Cell Biol* **16**, 356–363.

21 Kizuka Y, Tonoyama Y & Oka S (2009) Distinct transport and intracellular activities of two GlcAT-P isoforms. *J Biol Chem* **284**, 9247–9256.

22 Uemura S, Yoshida S, Shishido F & Inokuchi J (2009) The cytoplasmic tail of GM3 synthase defines its subcellular localization, stability, and in vivo activity. *Mol Biol Cell* **20**, 3088–3100.

23 Christiansen D, Milland J, Dodson HC, Lazarus BD & Sandrin MS (2009) The cytoplasmic and transmembrane domains of secretor type

alpha1,2fucosyltransferase confer atypical cellular localisation. *J Mol Recognit* **22**, 250–254.
24 Malagolini N, Santini D, Chiricolo M & Dall'Olio F (2007) Biosynthesis and expression of the Sda and sialyl Lewis x antigens in normal and cancer colon. *Glycobiology* **17**, 688–697.
25 Rabouille C, Hui N, Hunte F, Kieckbusch R, Berger EG, Warren G & Nilsson T (1995) Mapping the distribution of Golgi enzymes involved in the construction of complex oligosaccharides. *J Cell Sci* **108** (Pt 4), 1617–1627.
26 Nakamura N, Rabouille C, Watson R, Nilsson T, Hui N, Slusarewicz P, Kreis TE & Warren G (1995) Characterization of a cis-Golgi matrix protein, GM130. *J Cell Biol* **131**, 1715–1726.
27 Chia J, Goh G, Racine V, Ng S, Kumar P & Bard F (2012) RNAi screening reveals a large signaling network controlling the Golgi apparatus in human cells. *Mol Syst Biol* **8**, 629.
28 Linstedt AD & Hauri HP (1993) Giantin, a novel conserved Golgi membrane protein containing a cytoplasmic domain of at least 350 kDa. *Mol Biol Cell* **4**, 679–693.
29 Foulquier F, Amyere M, Jaeken J, Zeevaert R, Schollen E, Race V, Bammens R, Morelle W, Rosnoblet C, Legrand D *et al.* (2012) TMEM165 deficiency causes a congenital disorder of glycosylation. *Am J Hum Genet* **91**, 15–26.
30 Carvalho AS, Harduin-Lepers A, Magalhaes A, Machado E, Mendes N, Costa LT, Matthiesen R, Almeida R, Costa J & Reis CA (2009) Differential expression of alpha-2,3-sialyltransferases and alpha-1,3/4-fucosyltransferases regulates the levels of sialyl Lewis a and sialyl Lewis x in gastrointestinal carcinoma cells. *Int J Biochem Cell Biol* **42**, 80–89.
31 Smith PL & Lowe JB (1994) Molecular cloning of a murine N-acetylgalactosamine transferase cDNA that determines expression of the T lymphocyte-specific CT oligosaccharide differentiation antigen. *J Biol Chem* **269**, 15162–15171.
32 Roth J & Berger EG (1982) Immunocytochemical localization of galactosyltransferase in HeLa cells: codistribution with thiamine pyrophosphatase in trans-Golgi cisternae. *J Cell Biol* **93**, 223–229.
33 Roth J, Taatjes DJ, Lucocq JM, Weinstein J & Paulson JC (1985) Demonstration of an extensive trans-tubular network continuous with the Golgi apparatus stack that may function in glycosylation. *Cell* **43**, 287–295.
34 Colley KJ (1997) Golgi localization of glycosyltransferases: more questions than answers. *Glycobiology* **7**, 1–13.
35 Tu L & Banfield DK (2010) Localization of Golgi-resident glycosyltransferases. *Cell Mol Life Sci* **67**, 29–41.
36 Banfield DK (2011) Mechanisms of protein retention in the Golgi. *Cold Spring Harb Perspect Biol* **3**, a005264.
37 Bretscher MS & Munro S (1993) Cholesterol and the Golgi apparatus. *Science* **261**, 1280–1281.
38 Masibay AS, Balaji PV, Boeggeman EE & Qasba PK (1993) Mutational analysis of the Golgi retention signal of bovine beta-1,4-galactosyltransferase. *J Biol Chem* **268**, 9908–9916.
39 Machamer CE (1991) Golgi retention signals: do membranes hold the key? *Trends Cell Biol* **1**, 141–144.
40 Nilsson T, Slusarewicz P, Hoe MH & Warren G (1993) Kin recognition. A model for the retention of Golgi enzymes. *FEBS Lett* **330**, 1–4.
41 Teasdale RD, D'Agostaro G & Gleeson PA (1992) The signal for Golgi retention of bovine beta 1,4-galactosyltransferase is in the transmembrane domain. *J Biol Chem* **267**, 4084–4096.
42 Hathaway HJ, Evans SC, Dubois DH, Foote CI, Elder BH & Shur BD (2003) Mutational analysis of the cytoplasmic domain of beta1,4-galactosyltransferase I: influence of phosphorylation on cell surface expression. *J Cell Sci* **116**, 4319–4330.
43 Shaper NL, Mann PL & Shaper JH (1985) Cell surface galactosyltransferase: immunochemical localization. *J Cell Biochem* **28**, 229–239.
44 Schnyder-Candrian S, Borsig L, Moser R & Berger EG (2000) Localization of alpha 1,3-fucosyltransferase VI in Weibel-Palade bodies of human endothelial cells. *Proc Natl Acad Sci USA* **97**, 8369–8374.
45 Bonifacino JS (2014) Adaptor proteins involved in polarized sorting. *J Cell Biol* **204**, 7–17.
46 Giraudo CG & Maccioni HJ (2003) Endoplasmic reticulum export of glycosyltransferases depends on interaction of a cytoplasmic dibasic motif with Sar1. *Mol Biol Cell* **14**, 3753–3766.
47 Quintero CA, Giraudo CG, Villarreal M, Montich G & Maccioni HJ (2010) Identification of a site in Sar1 involved in the interaction with the cytoplasmic tail of glycolipid glycosyltransferases. *J Biol Chem* **285**, 30340–30346.
48 Young WW Jr (2004) Organization of Golgi glycosyltransferases in membranes: complexity via complexes. *J Membr Biol* **198**, 1–13.
49 Uemura S, Shishido F, Kashimura M & Inokuchi J (2015) The regulation of ER export and Golgi retention of ST3Gal5 (GM3/GM4 synthase) and B4GalNAcT1 (GM2/GD2/GA2 synthase) by arginine/lysine-based motif adjacent to the transmembrane domain. *Glycobiology* **25**, 1410–1422.
50 Schindelin J, Arganda-Carreras I, Frise E, Kaynig V, Longair M, Pietzsch T, Preibisch S, Rueden C, Saalfeld S, Schmid B *et al.* (2012) Fiji: an open-source platform for biological-image analysis. *Nat Methods* **9**, 676–682.
51 Potelle S, Dulary E, Climer L, Duvet S, Morelle W, Vicogne D, Lebredonchel E, Houdou M, Spriet C, Krzewinski-Recchi MA *et al.* (2017) Manganese-induced turnover of TMEM165. *Biochem J* **474**, 1481–1493.

Supporting information

Additional supporting information may be found online in the Supporting Information section at the end of the article.

Video S1. Dynamics of vesicles containing the long and the short isoforms, respectively.

Video S2. Dynamics of vesicles containing the long and the short isoforms, respectively.